SANDIA REPORT

SAND2000-0599
Unlimited Release
Printed March 2000

LDRD Report: Smoke Effects on Electrical Equipment

Tina J. Tanaka, Edward Baynes, Jr., Steven P. Nowlen, John Brockmann, Louis Gritzo, and Christopher Shaddix

Prepared by
Sandia National Laboratories
Albuquerque, New Mexico 87185 and Livermore, California 94550

Sandia is a multiprogram laboratory operated by Sandia Corporation, a Lockheed Martin Company, for the United States Department of Energy under Contract DE-AC04-94AL85000.

Sandia National Laboratories

Issued by Sandia National Laboratories, operated for the United States Department of Energy by Sandia Corporation.

Available to DOE and DOE contractors from
Office of Scientific and Technical Information
P.O. Box 62
Oak Ridge, TN 37831

Prices available from (703) 605-6000
Web site: http://www.ntis.gov/ordering.htm

Available to the public from
National Technical Information Service
U.S. Department of Commerce
5285 Port Royal Rd
Springfield, VA 22161

SAND2000-0599
Unlimited Release
Printed March 2000

LDRD Report: Smoke Effects on Electrical Equipment

Tina J. Tanaka
Fusion Technology Department

Edward Baynes Jr.
Nuclear Technology Programs Department

Steven P. Nowlen
Risk and Reliability Analysis Department

John Brockmann
Thermal/Fluids Engineering Department

Louis Gritzo
Reactive Processes Department

Christopher Shaddix
Industrial and Combustion Department

Sandia National Laboratories
P. O. Box 5800
Albuquerque, NM 87185-1129

Abstract

Smoke is known to cause electrical equipment failure, but the likelihood of immediate failure during a fire is unknown. Traditional failure assessment techniques measure the density of ionic contaminants deposited on surfaces to determine the need for cleaning or replacement of electronic equipment exposed to smoke. Such techniques focus on long-term effects, such as corrosion, but do not address the immediate effects of the fire. This document reports the results of tests on the immediate effects of smoke on electronic equipment. Various circuits and components were exposed to smoke from different fuels in a static smoke exposure chamber and were monitored throughout the

exposure. Electrically, the loss of insulation resistance was the most important change caused by smoke. For direct current circuits, soot collected on high-voltage surfaces sometimes formed semi-conductive soot bridges that shorted the circuit. For high voltage alternating current circuits, the smoke also tended to increase the likelihood of arcing, but did not accumulate on the surfaces. Static random access memory chips failed for high levels of smoke, but hard disk drives did not. High humidity increased the conductive properties of the smoke. The conductivity does not increase linearly with smoke density as first proposed; however, it does increase with quantity. The data can be used to give a rough estimate of the amount of smoke that will cause failures in CMOS memory chips, dc and ac circuits. Comparisons of this data to other fire tests can be made through the optical and mass density measurements of the smoke.

Acknowledgement

The authors would like to thank the two funding sources primarily involved in this work, the US Nuclear Regulatory Commission and the Laboratory Directed Research and Development program at Sandia National Laboratories. The authors would also like to thank the various students that participated on this project, Karla S. Waters, Paul Lucero, and Michael A. Dandini for their efforts in assisting with the smoke tests and data evaluation.

Contents

Figures

Tables

Summary

The immediate effects of smoke on electronics are different from the long-term effects of metal loss by corrosion, which has been studied by insurance companies to reduce losses of equipment. This report concentrates on the immediate effects, in particular the increase of conductance through the presence of smoke, because this change has been found to be the most harmful to electrical circuits. When smoke is present, the conductivity between air-insulated conductors will increase, and this can lead to shorts or arcs. For static electric fields as in the case of direct current (dc) circuits, the electric field attracts smoke, which deposits on contacts to form a bridge. Typical values of conductivity for smoke-bridged circuits are as low as 1 MΩ. For a high voltage alternating current circuit, ionized particles of soot provide a path for arcing. Smoke effects on capacitance and inductance were studied in earlier papers and found to be low.[1]

The goal of this project was to quantify how much smoke would be needed to cause a circuit or component to fail so that a model for the risk from smoke could be formulated. Finding a failure threshold for a particular circuit requires three types of information: how much smoke will cause a given loss of resistance, how much resistance loss can be tolerated by a circuit, and how does the electric field from the circuit modify smoke deposition. Failure thresholds are important in determining the reliability of equipment. In addition to the amount of smoke present, conductivity changes also depended on the amount of humidity present. Humidity levels above 60% have been found by others to contribute significantly to the conductivity of soot on surfaces. These effects were also observed here.

Modeling conductivity through empirical equations, however, can be difficult, because of the random nature of the smoke and soot produced. Smoke particle sizes vary, and some single particles can be large enough to short a small-featured component. Humidity increases the conductivity of the soot once the soot has formed on a solid surface. Hence all the variables needed to model the conductivity that would result from burning a given amount of fuel are not easily known and incorporated. This project has laid some groundwork for estimates of failure rates, but has not measured all of the parameters required to predict the conductivity that results from the presence of smoke.

Experiments included in this report on how smoke deposits for different electric fields and the resulting conductivity have shown that deposition is highly dependent on the electric fields. The experiments using the parallel plates and mass vs. conductivity boards especially show how the electric field determines smoke distribution. Even relatively low voltages, such as 50 V, will affect the distribution of the smoke. The distribution of smoke on surfaces then affects the conductivity of the smoke layer.

Nomenclature

μ	Micron
Ω	Ohm
A	Ampere (measure of current)
ac	Alternating current
CMOS	Complementary metal-oxide semiconductor
d	Plate separation distance
D_o	Optical Density
dc	Direct current
dV/dt	Time derivative of voltage
E	Electric field
EPROM	Erasable programmable read-only memory
HF	High frequency
Hz	Hertz (frequency in 1/s)
IPC	Institute for Interconnecting and Packaging Electric circuits
L	Liter
LDRD	Laboratory Directed Research and Development
PLCC	Plastic leadless chip carrier
PVC	Polyvinyl chloride (plastic used for insulation)
RH	Relative humidity (usually in %)
RMS	Root mean square (For example, root mean square voltage $=\sqrt{\int_0^T V^2 dt / T}$)
RTD	Resistive temperature device
s	Second
S	Siemens (1/Ohms), conductance measure
SIR	Surface insulation resistance
SRAM	Static random access memory
T	Period (s)
USNRC	United States Nuclear Regulatory Commission
V	Volt
Y	Admittance (1/impedence)

1 Introduction

1.1 Statement of problem

Smoke can cause electronic equipment to malfunction. Malfunctioning critical electronic equipment such as nuclear power plant safety systems and air traffic control tower communications systems can cause serious harm to public health and the environment. Because smoke can spread easily, it has the potential to affect many pieces of equipment at once, and defeat redundant safety systems. How likely is this to happen and how do we prevent it? Addressing the likelihood of failure is important in determining whether to attempt to prevent as much smoke exposure as possible.

Insurance companies have addressed the long-term effects of smoke on electronics as it relates to equipment replacement or recovery. Studies of long-term electronic equipment failure by Reagor[2] have determined important parameters in predicting whether electrical equipment must be replaced or can be recovered after a fire. The most important characteristic for long-term failure is the density of chloride and sulfide ions on the equipment surfaces. Another important factor is the humidity; higher humidity leads to more conductivity and corrosion.[3] Thus, it is important to reduce the humidity immediately after a fire and remove ionic compounds to reduce long-term equipment losses.

When electronics are exposed to smoke, the most likely immediate effect is that previously insulated surfaces become more conductive.[1] The loss of insulation occurs in two ways: (1) the smoke is formed of small charged particles that can attach to charged surfaces, building a coating that can eventually provide a semi-conductive bridge, and (2) soot that settles on a surface can form a semi-conductive layer between contacts separated by an insulator. The conductivity of this surface layer depends on its chemical and physical make-up and also on humidity. The overall effect of the increased conductivity is to short-circuit the electronics, causing failure in circuits that require high resistance between contacts.

One way to model the failure of electronics would be to calculate the amount of leakage current that would result from smoke or soot. The leakage current and resulting failure would be dependent on fuel, burning conditions, smoke transport, and equipment design. Smoke density, composition, and deposition patterns as well as relative humidity may all affect how smoke causes failures. Equipment design is also important because the electrical field generated by equipment can attract smoke particles and the failure of the equipment depends on whether the leakage current that results from smoke is significant when compared to the currents that flow when the circuits are in a normal environment.

This project was started to determine how smoke changes the conductive properties of normally insulating materials such as air and dielectric surfaces. Measurements

of conductivity of the smoke-laden air and surfaces could help determine how likely electronics will fail due to shorts.

Research on the effects of smoke on electronics at Sandia National Laboratories was started at the request of the US Nuclear Regulatory Commission (USNRC) in 1994 to determine the effect of smoke on microprocessor-based safety systems. Two reports have been published for the USNRC program, "Circuit Bridging of Components by Smoke"[4], and "Effects of Smoke on Functional Circuits".[1] A final report on smoke is to follow in the year 2000. In addition to this research, Oak Ridge National Laboratory has been researching the environmental factors that may affect microprocessor-based electronics and have included some experiments on a digital safety system exposed to smoke.[5]

2 Methods and materials

2.1 Smoke Production

To obtain information on conductivity, smoke tests must expose circuits to realistic, repeatable smoke conditions. Burning conditions can be highly variable—even the method of stacking fuel can influence the quality and quantity of smoke produced. To control as many conditions as possible, a smoke exposure facility was located in an environmental chamber that could be controlled for temperature and humidity. Humidity is an important parameter in the amount of leakage current that will be generated in electronics exposed to smoke.

The fuels that were burned include cable insulation, Douglas fir blocks, and jet fuel. These fuels represent common materials burned in accidental fires: plastic, cellulose, and petroleum products. Cable insulation materials vary in composition, depending upon their intended use. Because much of this work was funded by the USNRC, the majority of the fuels tested were cable insulation and most of the cables are qualified for use in the nuclear power industry. Because the focus was on effects on electronics rather than dependence on the burning of different insulation materials, a mixture of typical cables used in nuclear power plants were burned instead of individual cable materials. Because of the high level of interest in polyvinyl chloride (PVC) and its use in household wiring, PVC was also burned.

Heating the fuel with quartz lamps produced smoke. The smoke was channeled up through a chimney from the combustion chamber to the smoke exposure chamber. Figure 1 shows the smoke exposure chamber used to expose individual components. All of the smoke that was produced was contained within a Lexan exposure chamber. Thus, this was a static smoke test, as opposed to a dynamic test where fresh air is blown in to replace the smoke. To produce standard conditions, the quartz lamps were always turned on for 15 minutes, the components were always enclosed in the chamber for 1 hour, and the air in the exposure chamber was vented after 1 hour of exposure. The components and circuit boards were monitored before

each exposure and then throughout the test at regular intervals of 10 seconds, if possible. Monitoring continued after the smoke exposure for another hour.

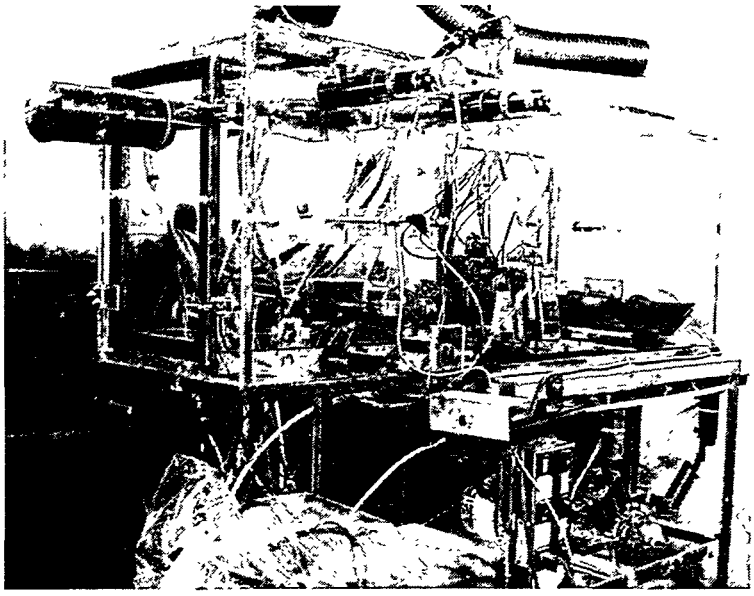

Figure 1. 200-L smoke exposure chamber.

2.2 Smoke measurements

The smoke conditions were measured using physical means: optical density, mass density of air samples, and the areal density (mass per surface area) of soot deposited on flat surfaces. Chemical analysis of the soot was performed before the LDRD program started and has identified several chlorides and sulfates as standard ionic by-products of the burning cables. No further chemical analysis was performed during the LDRD program because of the limited scope of work.

2.2.1 Fuel mass loss

Fuel mass loss indicates how completely a fuel is burned. In general, the higher the heat flux, the faster and more completely the fuel is burned. Fuel mass was tracked by two methods, the fuel in a tray was weighed before and after each test, and a low-resolution measurement was made during the test using a load cell. A drawback of the load cell method was that the load cell was temperature-sensitive so measurements during the flaming period, when the lamps were on, were not very accurate.

2.2.2 Optical density

Optical density was measured with a He-Ne laser system. The laser beam was split and part of the laser light was monitored with a silicon photodiode detector while the rest of the laser light was collimated onto a fiber optic bundle. The fiber bundle directed the laser light through the smoke enclosure, and then a second fiber optic bundle directed the light back to a second silicon photodiode detector. The

transmission through the chamber was measured by comparing the signals from the monitor detector and the transmission detector. Since the objective was to measure the smoke in the air, nitrogen gas was used to purge the smoke from optical surfaces in the smoke chamber. The optical density, D_0, was then calculated using the Lambert-Beer law:

$$D_0 = -\ln(\frac{I}{I_0})\Big/t .$$

The ratio of I/I_0 is the ratio of the light transmission intensity while the smoke is in the chamber to the light transmission intensity before the smoke is added to the chamber, and t is the distance the beam passes through the smoke (10 cm).

2.2.3 Mass density

During the smoke exposure, four samples of air were drawn through silver membrane filters to measure the smoke mass density. The filters were weighed before installation and again after the smoke exposure. The filters had a 0.8 μ effective pore size. The amount of air filtered to obtain the samples on the filters was determined by measuring the airflow through the filters before and after the smoke test. Each sample was drawn for 30 s at rates less than 10 L/min (0.166 L/s), and the sample was taken from the air just above the optical density measurement. Comparisons between the optical density and the mass density helped ensure that the amount of smoke was known and could be compared with fire modeling codes.

2.2.4 Mass deposition

The mass of the deposited soot was measured with a quartz crystal microbalance. A quartz crystal, patterned with gold contacts was connected to an oscillator circuit that drives the crystal at its resonant frequency. When smoke deposits on the surface, the resonant frequency decreases (as in mass loading of a spring), and the mass can be measured as the test is run. The disadvantage of this device is that the temperature changes the resonant frequency of the quartz; therefore, corrections had to be made for temperature changes. Although the crystal is an AT-cut quartz with a stable frequency for temperatures around 20ºC, at 40ºC, which was the temperature of much of the test, the frequency response is highly temperature dependent. Also, soot does not deposit on all surfaces equally; temperature and surface polarities are known to determine soot deposition. Hence measurements on these quartz/gold surfaces may not be indicative of how much smoke deposits on other types of surfaces, such as printed circuit boards. Uncertainty in how well agglomerated soot particles couple to the surface can also introduce uncertainty in this measurement.

2.2.5 Humidity measurements

The conductivity of soot is highly dependent on the relative humidity (RH) in the smoke chamber. The smoke exposure tests at Sandia National Laboratories were

performed with no control over the humidity other than the beginning and the end of the smoke test. Because conductivity depends on humidity and is a major concern in the reliability of electronics, humidity can be an important parameter to measure during a test.

Near the end of the program period, small RH gages were included in the smoke chamber, one near the electronics under test and one near the mass vs. conductivity measurement boards. To reduce the likelihood of damage to these gages, a new gage was installed for each smoke test. A comparison of the exposed gages to new the main environmental chamber humidity gages showed that the exposed gages registered 2% less RH. The gages include a platinum resistive temperature device (RTD) so that both RH and temperature can be measured and other measurements of humidity can be derived. Figure 2 shows the relative humidity/temperature gage that was placed in the smoke chamber to give readings throughout the smoke exposure. Relative humidity is the ratio of the amount of water vapor in the air to the amount of water vapor in saturated air. Another important factor to be derived from this is the mixing ratio, the ratio of the amount of water to the amount of dry air as a result of burning fuel.

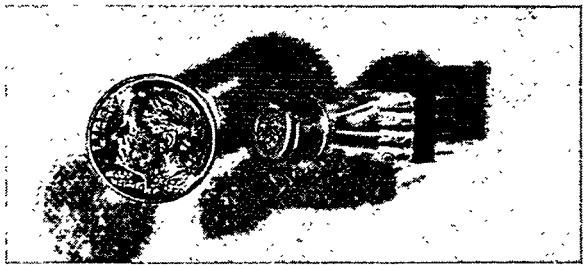

Figure 2. Humidity/temperature gage included in the smoke exposure chamber.

2.2.6 Temperature measurements

The temperature and humidity of the smoke chamber were controlled before and after the smoke exposure, but during the fire and for 45 minutes after the fire while the smoke was contained in the chamber, the temperature and humidity were uncontrolled. The temperature within the smoke exposure chamber was measured throughout with type K thermocouples. The thermocouples were located in seven positions inside of the smoke chamber and three outside of the chamber.

2.3 Electrical measurements

Two types of leakage currents have been measured: the leakage between two freestanding vertical parallel plates (Figure 3) and the leakage between interdigitated comb patterns printed on a circuit board.

Figure 3. Perforated parallel plates.

2.3.1 Parallel plates (DC and HF)

The parallel plate conductivity was measured to determine if the smoke in the air was causing increased conduction. The plates were spaced 2.5 mm apart and were made of perforated stainless steel. The perforations allowed more transport of smoke to the region between the plates. Four pairs of plates were placed in the smoke chamber at a time and each was biased with a different voltage: 500 Vdc, 50 Vdc, 5 Vdc, and 1 Vac. The plates biased with dc voltages were connected electrically in series with a resistive circuit that allowed for measurement of leakage currents across the plates. The ac-biased plates were connected to a network analyzer, which measured the admittance of the plates for a range of high frequencies between 0.5 and 30 MHz.

2.3.2 Parallel plates (AC)

AC voltage was applied to parallel plates made of perforated stainless steel. The steel plates were 5×7.5 cm^2 in area and spaced between 3 and 25 mm apart for the tests. The plates were mounted near the top of the smoke chamber. 4.2 kV (RMS) at 60 Hz was applied to the plates. Arcing was measured with a Pearson current probe on the high voltage conductor, and the voltage was measured with a two-channel oscilloscope. Both the current and voltage waveforms were recorded when the plates arced. Some preliminary measurements of shorting voltage vs. humidity in the chamber showed little variation due to humidity.

Ideal parallel plates are infinite in extent and perfectly flat. For ideal parallel plates, the field between the plates should decrease linearly with increasing separation. In our tests, plate separation was a significant factor in likelihood of arcing, although the variation was not linear. To study this, the voltage was raised slowly until the plates began to arc, then another separation distance was selected

and the voltage raised again. When the plates began to arc, the arcing tended to be continuous. The ac power supply could supply up to 40 mA of current on a continuous basis, but if required to provide more, the voltage would drop. The arc current was high enough to lower the potential across the plates. Nevertheless, the arcing continued once a path was established because the hot, ionized air provided an easier path for arcing than normal.

2.3.3 Surface insulation resistance (SIR)

Interdigitated comb patterns were placed in the chamber either face up and parallel to the ground or vertical and perpendicular to the ground. The comb patterns, shown in Figure 4, were connected to a resistive circuit similar to the dc parallel plate circuits, biased with 5 Vdc, and leakage currents were monitored in these circuits. These patterns (IPC-B-24 boards), developed by the Institute for Interconnecting and Packaging Electronic Circuits, measure surface insulation resistance and are used by the IPC to monitor the accuracy of the printed circuit manufacturing process.[6] Better processing yields lower SIR values. Smoke and other contaminants increase SIR values. Humidity can influence contaminated boards.

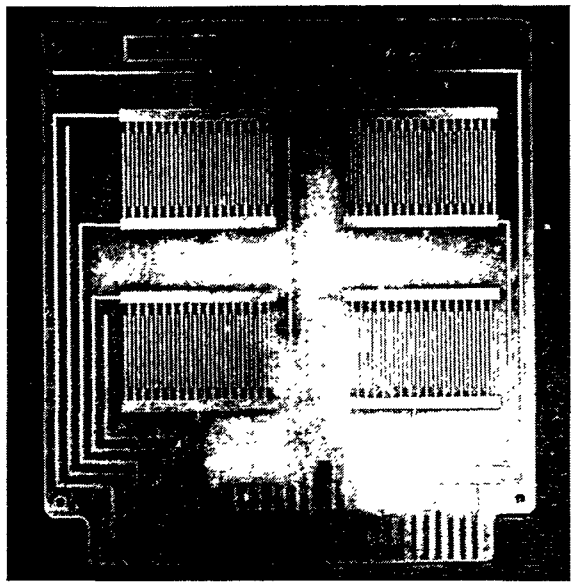

Figure 4. Interdigitated comb pattern, IPC-B-24.

2.3.4 Mass vs. conductivity measurements

An interdigitated pattern was designed for use as a surface to collect smoke for weighing and comparison to conductivity. The pattern has solder traces separated by 0.1" (0.25 cm). The pattern is illustrated in Figure 5. Printed circuit boards with these traces were biased with 5, 50 and 500 Vdc and leakage currents were measured as they were exposed in smoke. The substrate for these printed circuit boards was very thin so that the weight of the boards was below 1 g, but each printed circuit board had 30 cm^2 of surface area. The printed circuit boards were

weighed before and after each smoke exposure to determine how much smoke would cause a given amount of shorting. All boards were placed in a horizontal position to get the maximum collection of soot possible.

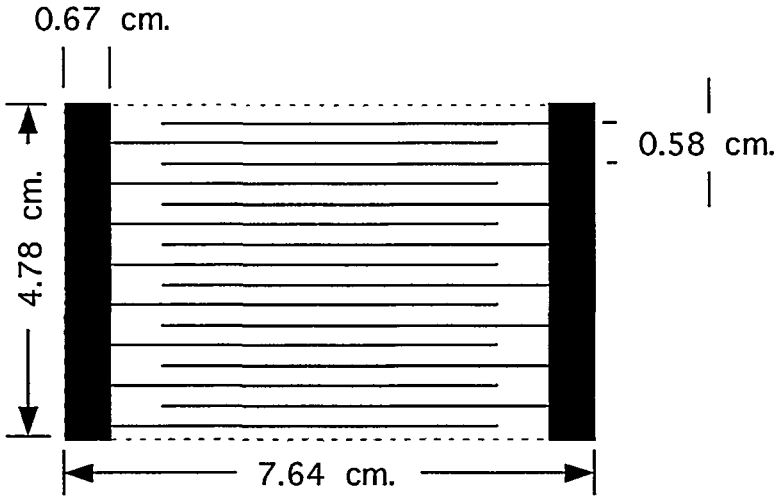

Figure 5. Mass vs. conductivity board pattern.

2.4 Component testing

Leakage current measurements by themselves do not indicate whether a circuit will fail. Failure depends on the type of circuit and expected operating parameters. To determine whether certain circuits will fail, we included several operating circuits in the tests.

2.4.1 Digital Throughput

The connectors typically used for serial signal transmission, parallel signal transmission, and Ethernet transmission for standard personal computers are the D-subminiature 9-pin (DB-9), the D-subminiature 25-pin (DB-25), and the network modular (RJ-45) connectors, respectively. To test these connectors, signals from a personal computer were routed through connectors placed in the smoke exposure chamber. A printed circuit board was manufactured that would wire three pairs of connectors (a pair of each type) so signals entering from one connector would be transmitted straight through to its pair. All of the connectors were through-hole-soldered connectors. The printed circuit board was placed in the smoke chamber so those through-hole pins were uppermost, exposing the contacts to the most smoke deposition. Figure 6 shows the digital throughput board with typical connectors used for signal output.

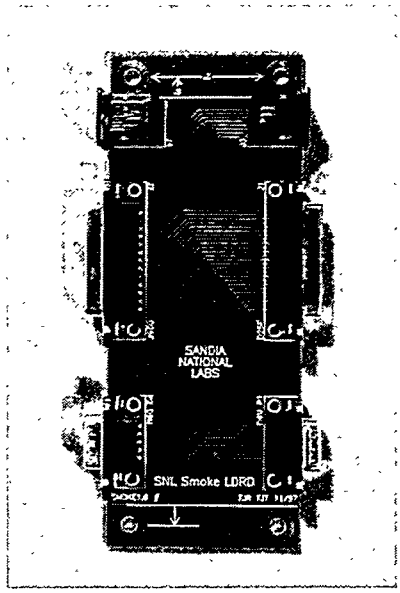

Figure 6. Throughput boards for testing transmission connections.

To test the connectors, appropriate digital signals were transmitted through the connectors in the smoke chamber. For serial communication, a bit-error rate test was performed on a serial communications port on a personal computer. To test parallel communications, an IOMEGA Zip drive was placed at the end of a parallel port connection after the connecting cable was passed through the smoke chamber. Data were written to and read from the Zip drive, located outside of the smoke chamber. To test Ethernet communications, the network communications between two computers were monitored as data was transmitted between computers.

2.4.2 SRAM and EPROM memory chips

Two types of memory chips were tested: static random access memory (SRAM) and erasable programmable read-only memory (EPROM). The memory chips were mounted on a printed circuit board and tested with a chip analyzer that tested the chips for some standard operations. The SRAM chips were 128K x 8 bit complementary metal oxide semiconductor (CMOS) memory chips: MCM6226BBEJ20 (biased with 5 Vdc) and MCM6926A (biased with 3.3 Vdc). The EPROM chips were AM27C256 in two different packages, the 28-pin dual-in-line (DIP) package, and the 23-pin plastic-leadless chip carrier (PLCC). The EPROM chips were programmed prior to installation on a printed circuit board. These chips are shown in Figure 7.

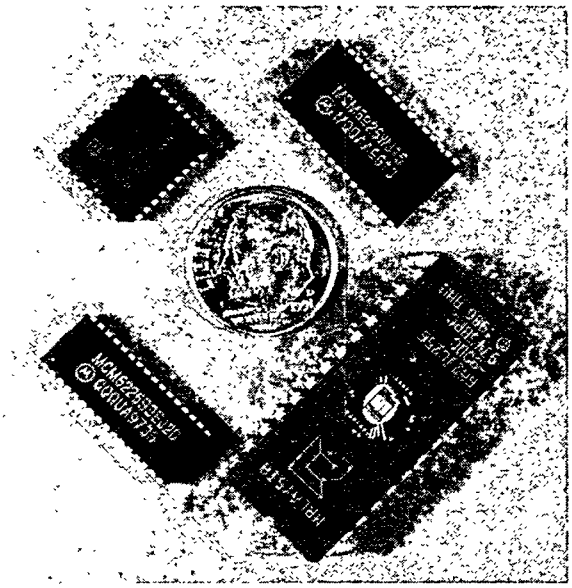

Figure 7. Tested SRAM and EPROM memory chips.

Two types of tests were performed on the chips in the smoke chamber: functional and timing tests and parametric measurements. The functional and timing tests measure if the chip can record and output data from all cells in the memory chip without errors and indicate how long the chip takes to make data available. Parametric measurements test to see if certain parameters change as the chip is exposed to smoke. The parametric measurements include a standby current measurement (current drawn by the supply voltage pin), a current leakage measurement (a standard voltage is applied to the pin and the current measured), and current injection test (a standard current is injected and the voltage level measured). Two chips were exposed to the smoke at a time, and all of the chip tests were repeated at 30-s intervals.

2.4.3 Hard disks

Hard disks are standard equipment in most personal computers. When hard disks fail, the entire computer can halt, waiting for the next instruction to execute. A series of smoke exposures were performed on standard, 8.4 Gbyte hard drives.* These hard drives are not vacuum-sealed, but have a very good adhesive tape seal. The hard drive was placed inside of the smoke chamber while the computer was placed just outside of the smoke chamber with an 18" (46 cm) data cable. Data were written to and from the hard drive and comparisons of the data read and written were made to determine if the smoke caused any failures. The hard drive was placed upside down to its standard orientation because more electronic circuitry would be exposed to the smoke in this orientation.

---

* Western Digital Caviar 28400 drive

2.4.4 Non-Volatile SRAMs

One test not completed with the end of the LDRD period is the test of the non-volatile SRAM. Dallas Semiconductor manufactures a non-volatile SRAM, which contains a lithium backup battery. This SRAM will store data even if the main power supply drops for up to 9 years. Power must be applied to read from or write to this chip, but data are not lost when power is absent. This chip was not tested as extensively as the SRAM and EPROM in section 2.4.2. The function and the power supply current were monitored, but not all of the other current and voltage measurements used in the earlier SRAM tests were monitored. Like the other SRAM and EPROM chips tested earlier, non-volatile SRAMs are based on CMOS technology.

3 Results

The smoke exposure tests yielded many interesting results. One of the most important results was identification of the mechanism by which charged parallel plates will conduct in a smoke environment. Others results deal with the effect of smoke on high voltage ac and the simultaneous effect of smoke and humidity.

3.1 Optical vs. mass density

Optical density was measured in the smoke chamber with a He-Ne laser. The mass density was measured just above the laser measurement by pumping air from the smoke chamber and passing it through silver membrane filters. Figure 8 shows that the optical density was proportional to the mass density of the smoke. These measurements were made for several different fuels, as shown in Table 1.

Table 1. Ratio of Optical Density to Smoke Mass Density

Fuel	Optical Density/Mass density (L/mg-cm)
PVC	0.038
Ground mixed cable	0.026
Brand rex cable	0.022

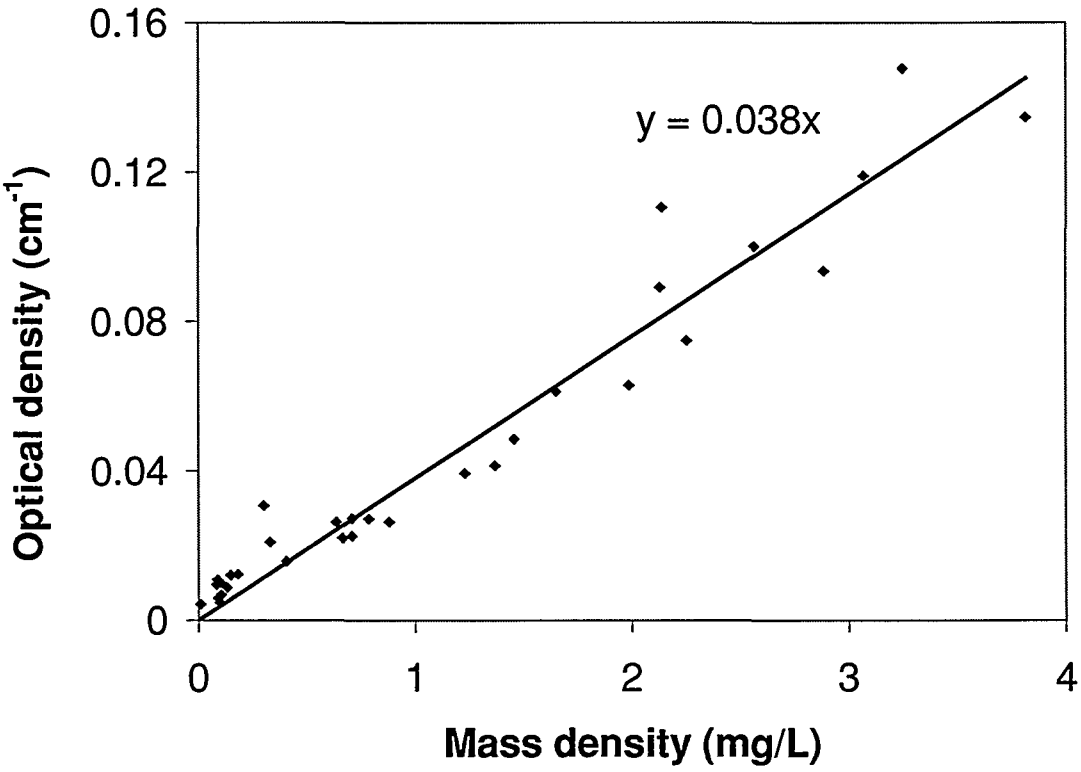

Figure 8. Optical Density vs Mass density for PVC smoke.

3.2 DC potential and HF on parallel plates

A surprising result was that the conductance between parallel plates remained high after the smoke concentration, as measured by optical density in the smoke chamber, dropped drastically following the "smoke peak", indicating that there was very little smoke in the air. This result is plotted in Figure 9 for a 500 Vdc-biased pair of plates. A video recording of the plates in the smoke chamber shows the mechanism by which this occurs. Four frames from this recording are shown in Figures 10–13. The smoke was attracted to high-voltage surfaces and built up fragile bridges between the parallel plates. These carbonaceous bridges conducted current much like carbon resistors. When the air was forcefully vented from the smoke exposure chamber, the carbon bridges were destroyed and the conductivity fell. While smoke was in the air, air movement destroyed some of the bridges, but more smoke was then attracted to the bridge formation. After the optical density dropped, however, there was no more smoke to replace the bridges and the conductance slowly fell.

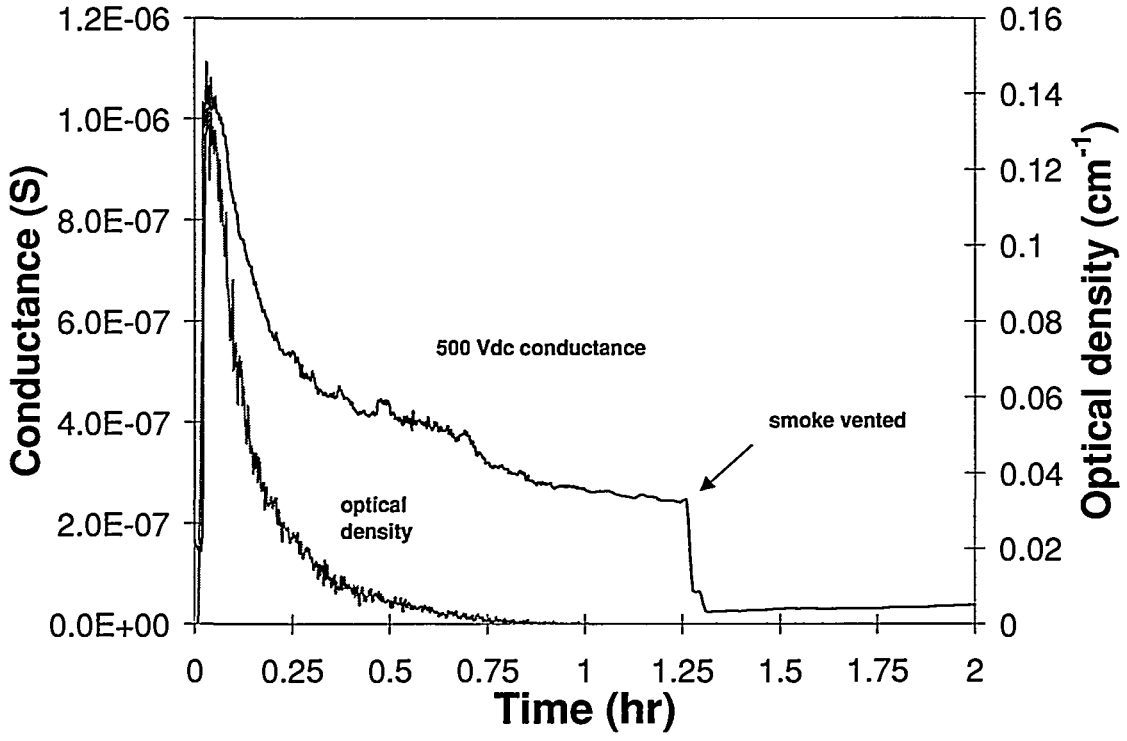

Figure 9. 500 Vdc Conductance and Optical density vs. time.

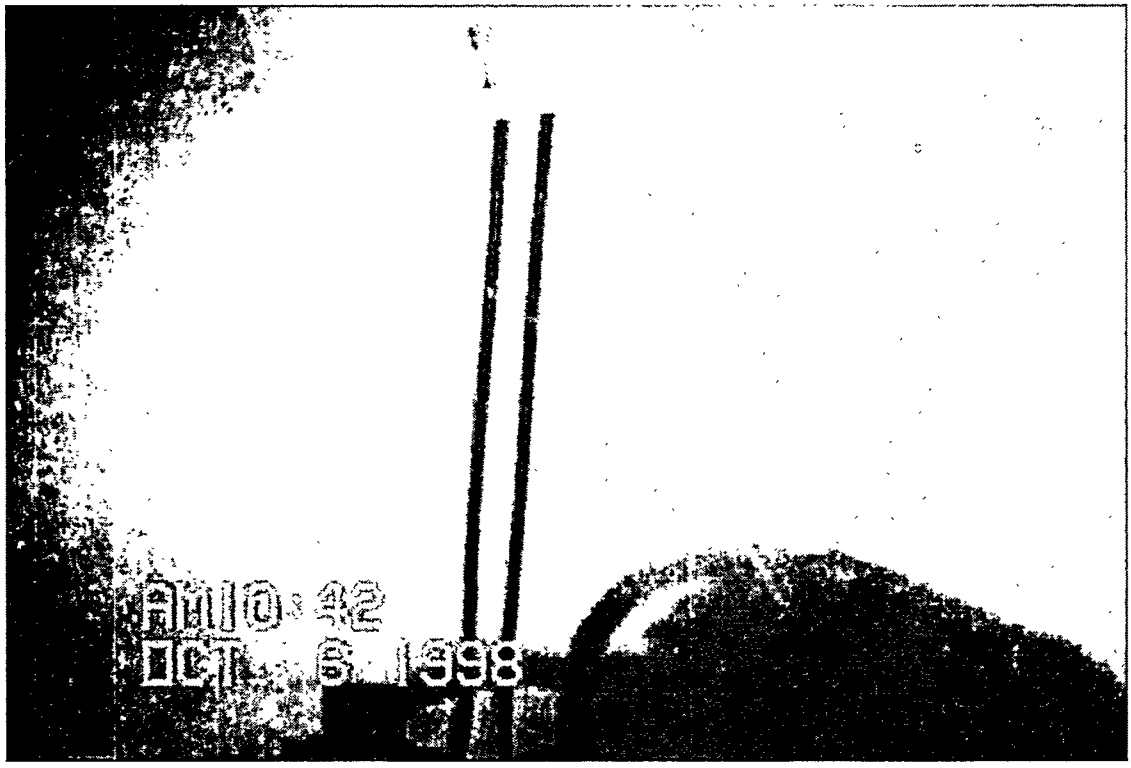

Figure 10. 500 Vdc parallel plates at beginning of test.

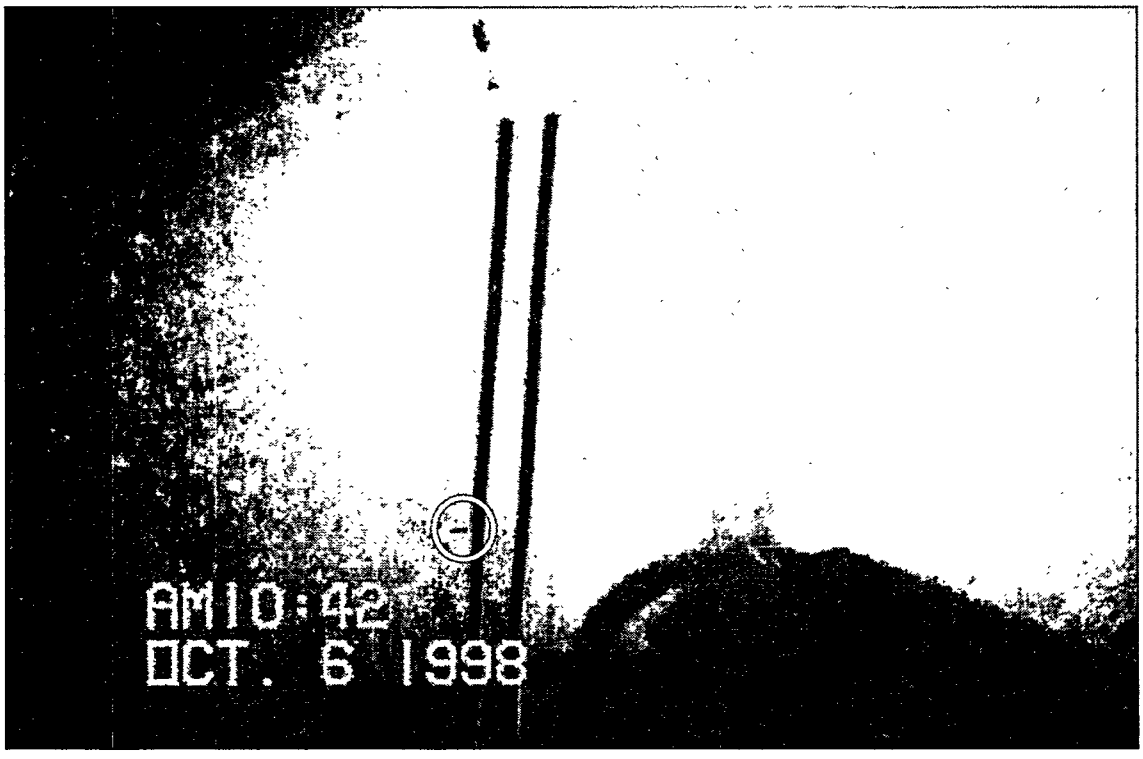

Figure 11. 500 Vdc parallel plates with a small amount of smoke, note whisker of soot, encircled, on left-hand plate.

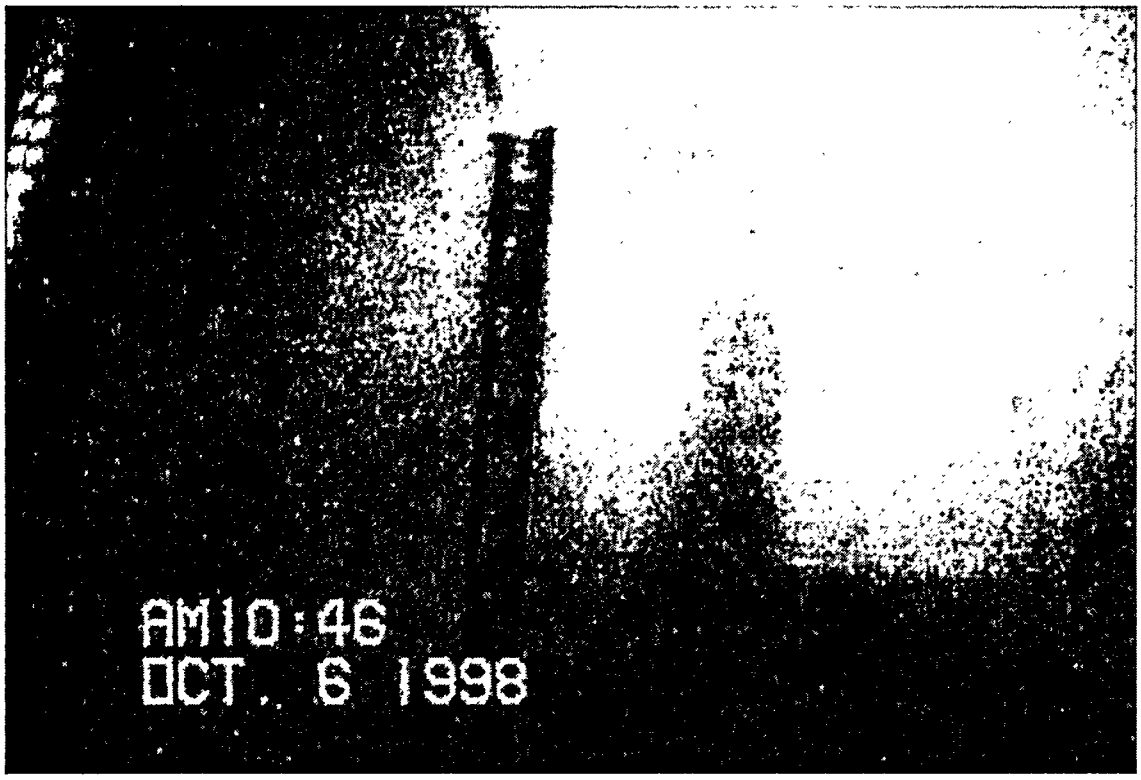

Figure 12. 500 Vdc parallel plates, 4 minutes into smoke test.

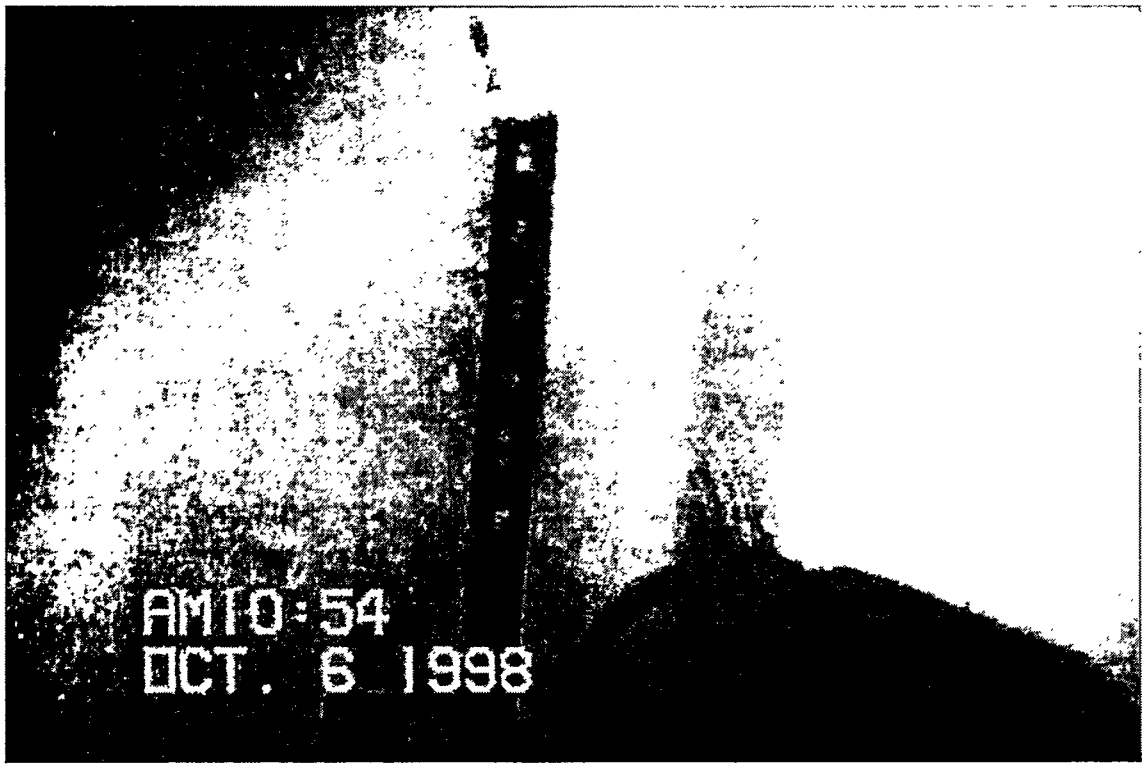

Figure 13. 500 Vdc parallel plates after 12 minutes of smoke exposure.

A lot of soot collected on these plates; they tended to act like electrostatic precipitators and attracted soot particles. The soot was probably not evenly

distributed in the smoke chamber because high potentials attracted so much of the soot. Further discussion of these phenomena is in section 3.4. For the parallel plates, smoke to the right of the pair of plates was subject to one polarization of the electric field and the smoke to the left of the plates to the opposite field. The field strength was large in the general area and smoke was attracted to the plates. More soot should be attracted to the parallel plates when the voltage is high.

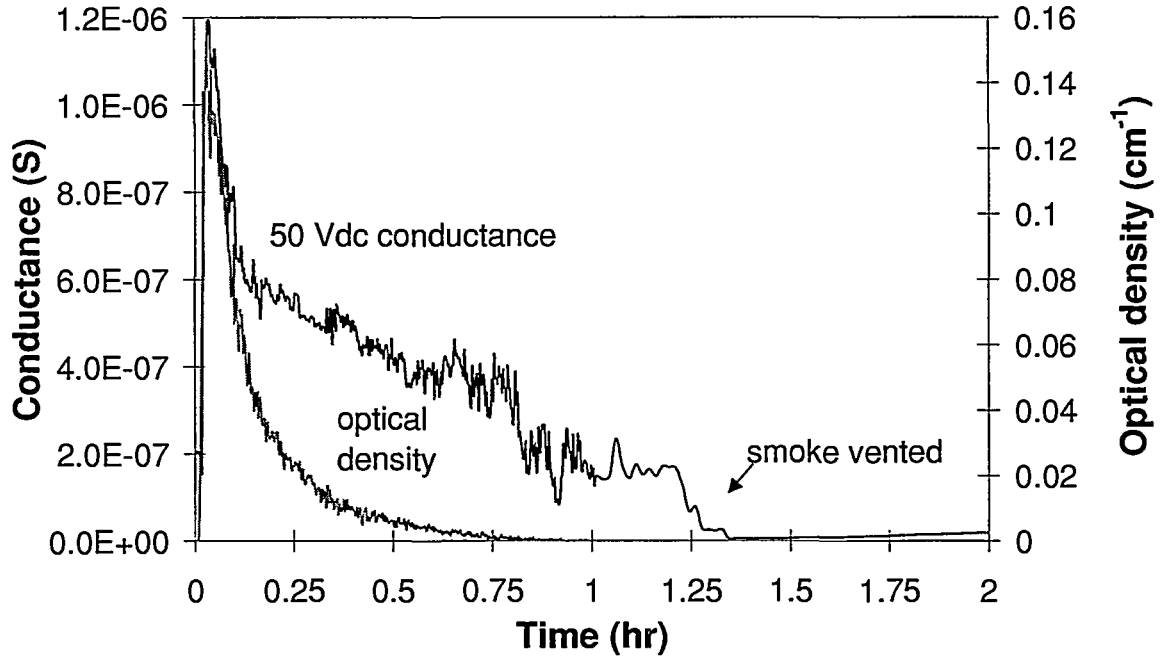

Figure 14. 50 Vdc parallel plate conductance and optical density vs. time.

The conductivity of the 50 Vdc-biased plates peaked when the optical density was highest, but did not drop as fast as the optical density (Figure 14). The conductivity on the 50 Vdc-biased plates was approximately the same as that on the 500 Vdc-biased plates at the peak of the smoke output (Figure 9); however, the 500 Vdc bridges were more robust. Higher voltages have more force to maintain the bridges, but since the plates were the same size, the peak conductivity was similar because a maximum volume of soot could be attached to each plate. The plate size might have limited the amount of soot volume that could be attached to each plate. The 5 Vdc-biased plates showed little increase of conductivity and probably did not have a strong enough field to attract soot and bridge the plates.

The high frequency measurements yielded a change in admittance as the smoke was added. At high frequencies the changes were larger than for low frequencies. Figure 15 shows the change in admittance as smoke was added for the same test as plotted in Figure 9 for 30 MHz. The parallel plates were set 2.5 mm apart. Smoke particles are semiconductive so the response of the circuit to smoke should be similar to the introduction of dielectric material between the parallel plates.

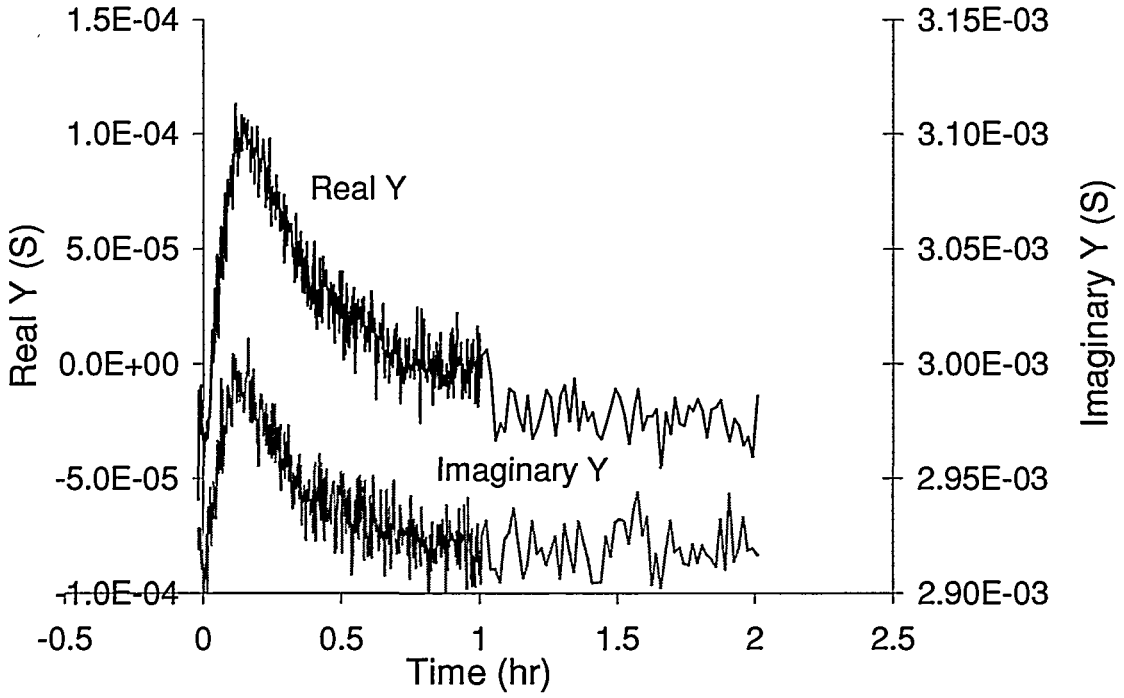

Figure 15. Real and imaginary parts of admittance at 30 MHz.

For a parallel plate capacitor, the capacitance is expressed as $C = \varepsilon A/d$ where A is the area of the plates, d is the distance between plates, and ε is the dielectric constant. Considering the resistance between two parallel plates, $R = d/\sigma A$ where σ is the conductivity of the air. These two formulas contain the geometric factor, A/d. Since the parallel plates used in our experiments are perforated, the electric field lines will not yield the standard values of capacitance and resistance. However, we can assume that the field lines will be equivalent for the two formulations and hence, a geometric factor g can be considered to be the same for both, i.e., $C = \varepsilon g$ and $R = 1/(\sigma g)$.

The geometric factor can be determined when there is no smoke in the air. In that case, $\varepsilon = \varepsilon_0$ or the electrical permittivity of air, 8.85×10^{-12} F/m. Thus, for a given capacitance measured in the air, C, can be determined. If the parallel plate can be modeled as a capacitor and resistor in parallel, the current from such a circuit would be: $I = V/R + C\,dV/dt$, where V is voltage and I is current. If we assume that $V = V_0 e^{j\omega t}$, a sine wave, then $I = V/R + j\omega CV$. Because the admittance, $Y = 1/V$, then $\mathrm{Re}(Y) \equiv G = 1/R = g\sigma$ and $\mathrm{Im}(Y) \equiv B = C\omega = \varepsilon g\omega$. Thus, the real part of the admittance gives the conductance while the imaginary part is proportional to capacitance.

3.3 AC potential on parallel plates

Smoke caused increased arcing. Figure 16 shows the amount of fuel available to burn, and parallel plate separation, for each of the test results. Both the amount of fuel that was burned and the separation of the parallel plates determined whether the smoke would cause arcing. If the electricity started to arc, arcing began immediately with the introduction of smoke. For some tests, arcing began when the smoke was added and continued until the power was turned off (1 hour). For other tests, only one or two arcs occurred; these are shown on the chart below as intermittent arcs. For tests at larger separation, no arcs occurred.

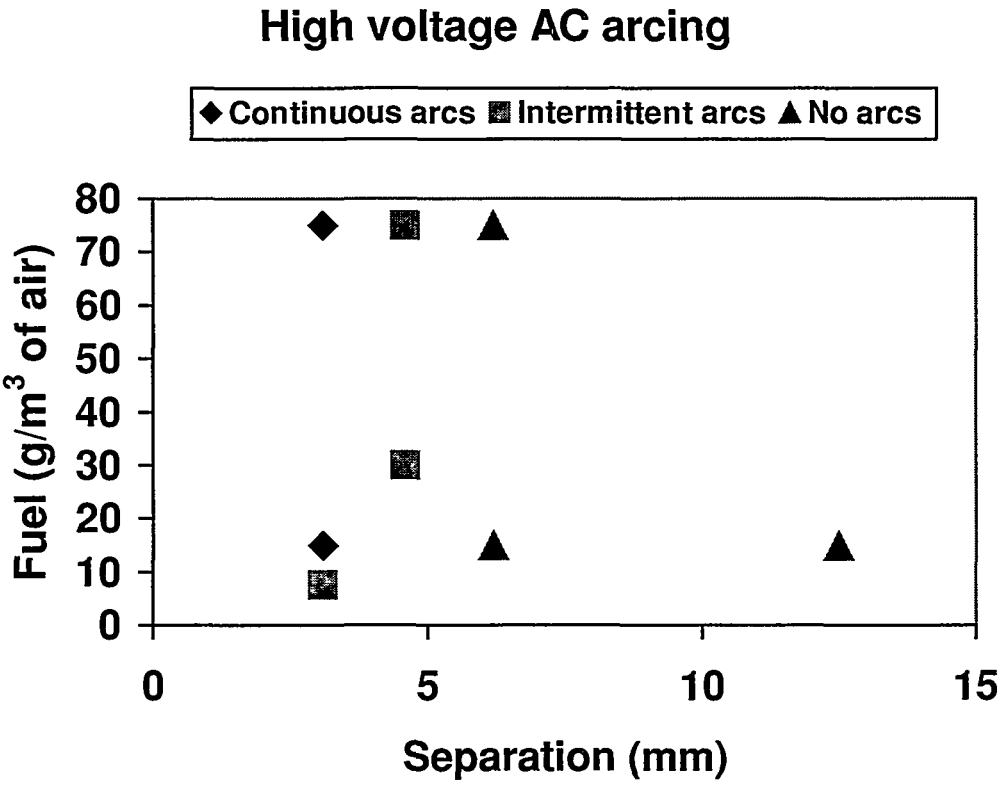

Figure 16. Results of high voltage ac smoke tests.

The electric field for ideal parallel plates is dependent on their separation and applied voltage. The field (E) is inversely related to the plate separation (d) and is proportional to the applied voltage (V):

$$E = V / d$$

The higher the electric field, the more likely an arc will form. Figure 17 shows the measured breakdown voltage for different separation distances, d. If the parallel plates were ideal plates, the data should fall on a straight line through zero.

Because the plates were perforated, were not perfectly straight, and were of limited extent, the equation does not fit perfectly.

Electrical arcs can be instigated by a random event (cosmic rays that ionize the gas between the plates, for example) and can continue if the conditions are correct because the arc ionizes the air and makes a more favorable condition for arcing to continue. Once arcing started, it continued even if the potential was lowered. Lightning strikes also create a similar phenomena; the ionized air along the first arc path is the path of least resistance for subsequent strikes and several strikes occur in quick succession.

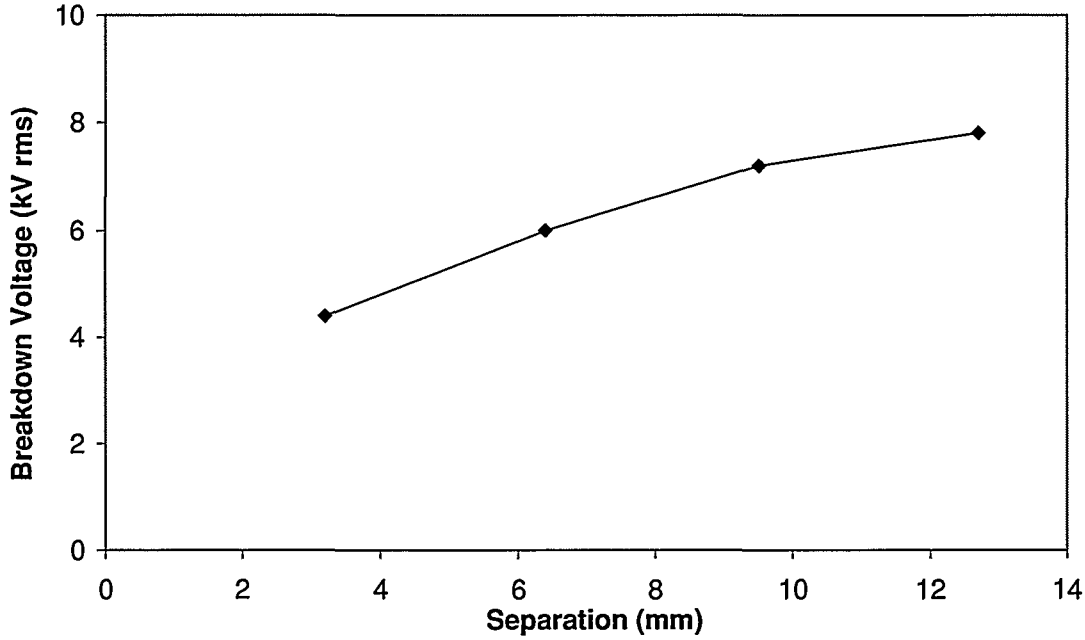

Figure 17. Breakdown voltage vs. plate separation.

The parallel plates formed a simple capacitor, so when the plates arced, the circuit oscillated with a frequency that was determined by the capacitance of the parallel plates and resistance of the circuit. Figure 18 shows the current during an arc. The frequency of the oscillation, 3.2 MHz, is much higher than the 60 Hz frequency of the potential applied to the parallel plates. Instead, this frequency is indicative of the inductance and capacitance of the parallel plates and cabling circuit.

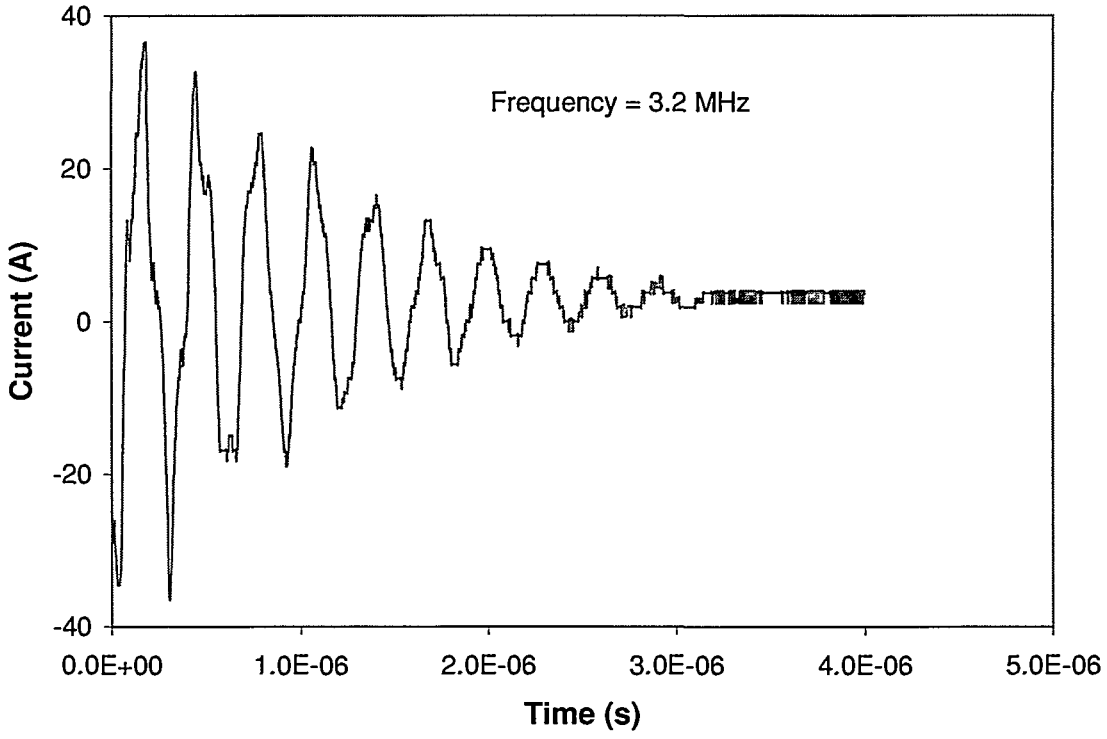

Figure 18. High voltage AC leakage current.

3.4 Smoke deposition vs. conductivity

The pattern of smoke deposition on the mass vs. conductivity boards depended on the applied bias voltage. As shown in Figure 19, 500 V and 50 V biased boards collected soot around the conductors, while the 5 V biased board had a more even distribution. On the 500 V-biased board, the area between conductors had little smoke deposition. Likewise, the 50 V biased board had a smaller area of little deposition. The higher the bias voltage, the more uneven the smoke deposition. The higher-biased patterns had stronger electric field strengths. A strong electric field exerts more force on the smoke particles, moving them towards the conductors. Hence, the higher-biased patterns had an accumulation of soot around the conductors.

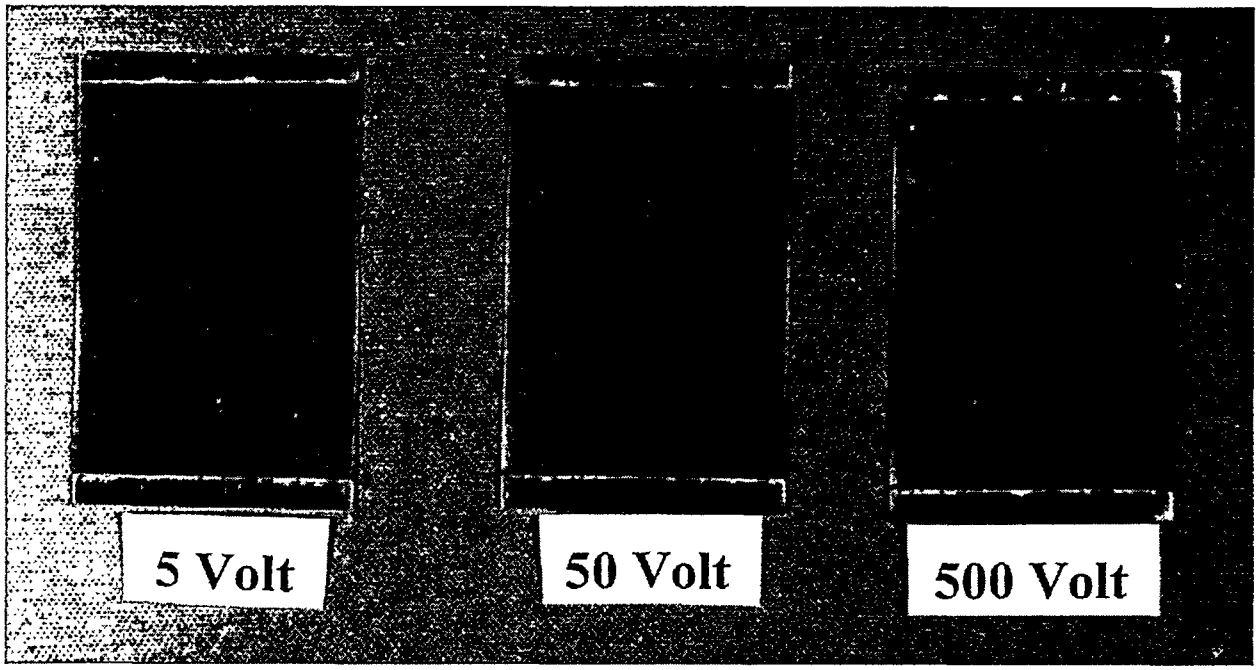

Figure 19. Mass vs. conductivity board from smoke test with 30 g of mixed cable.

The conductance between traces varied throughout the smoke test as shown in Figure 20. The conductivity was highest when smoke was in the air 3-4 minutes after the test started. After most of the smoke had settled or vented, the conductivity dropped more for the 500- and 50-V biased boards than the 5-V biased board. The higher conductivity of the 5-V biased board after 1 hour (the smoke was vented from the smoke chamber by then) could be attributed to the more even distribution of smoke on that board.

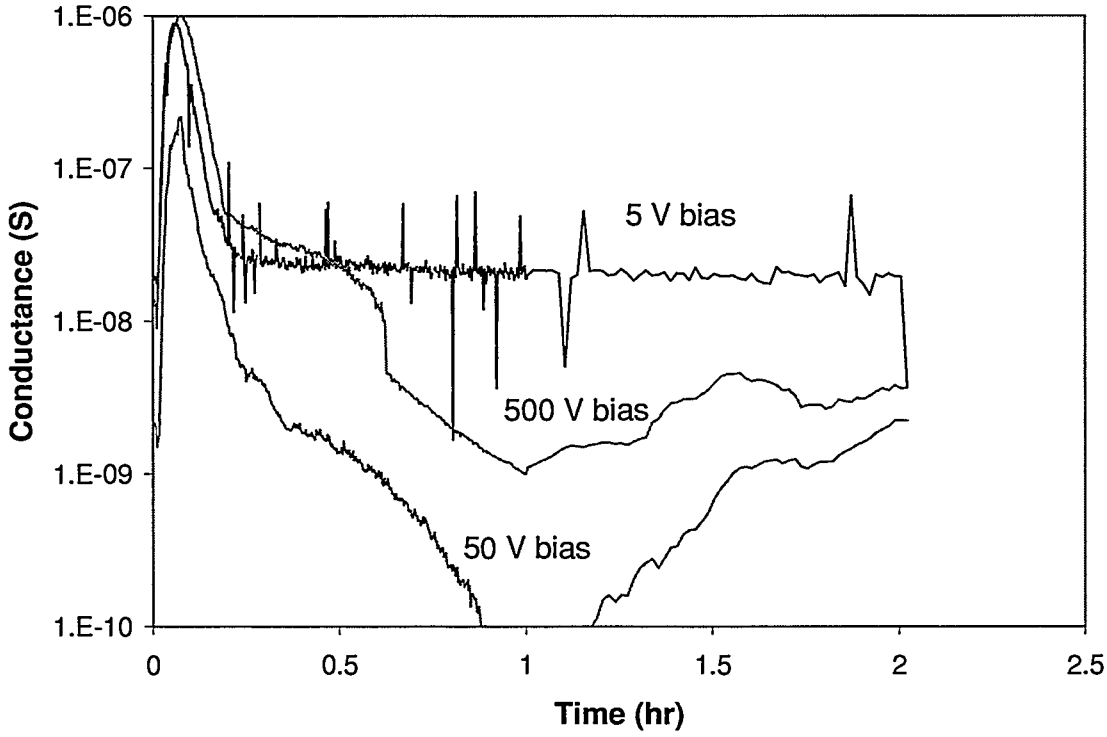

Figure 20. Comparison of the conductance between boards with different bias voltages.

Figure 21 compares the mass of deposition between boards for different amounts of fuel burned and at different bias voltages. The mass of smoke deposited does not vary significantly with the bias voltage. Although higher electric fields are present near the surface of the boards when the bias voltage is higher, the effect of the stronger electric field is cancelled far away from the boards, because there are an even number of traces on the circuit board. However, the smoke mass collected on the board varies with the amount of fuel burned. When more smoke is in the air, more smoke is deposited. As found in earlier experiments, no temperature effect was expected for the range of temperatures generated in the smoke chamber.[4]

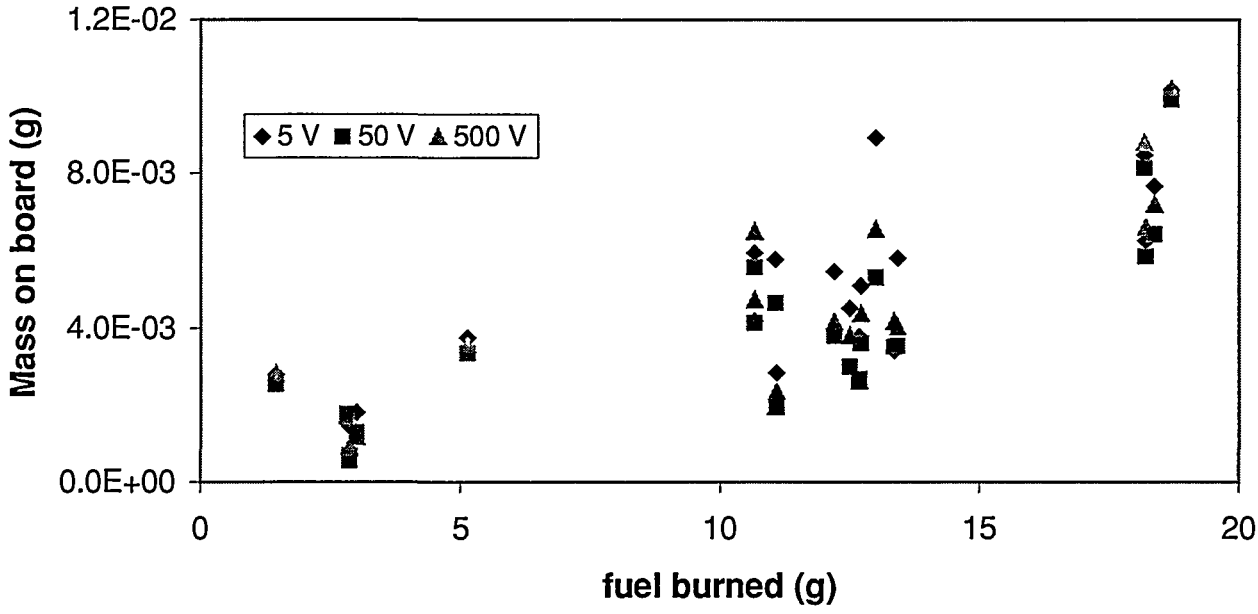

Figure 21. Smoke collected by conductivity board vs. amount of fuel burned.

The mass of soot collected on the conductivity boards related well to the amount of fuel burned, but not to the conductivity at times close to the end of the smoke exposure. This behavior may be attributed to dependence of conductivity on the relative humidity. This effect is discussed in the next section (3.5)

3.5 Effect of humidity

At the beginning of the smoke test, the humidity level is controlled by the environmental chamber, which surrounds the smoke exposure chamber, to approximately 75% RH. As the radiant heat lamps are turned on, the air in the smoke chamber is heated (Figure 22). The relative humidity decreases with increase of air temperature because hot air sustains more water vapor at saturation than cool air (Figure 23). Dry nitrogen is also added to the air near the smoke opacity measurement throughout the test. The dry nitrogen is used to sweep smoke from the air in front of the optics and keep lenses clear of soot.

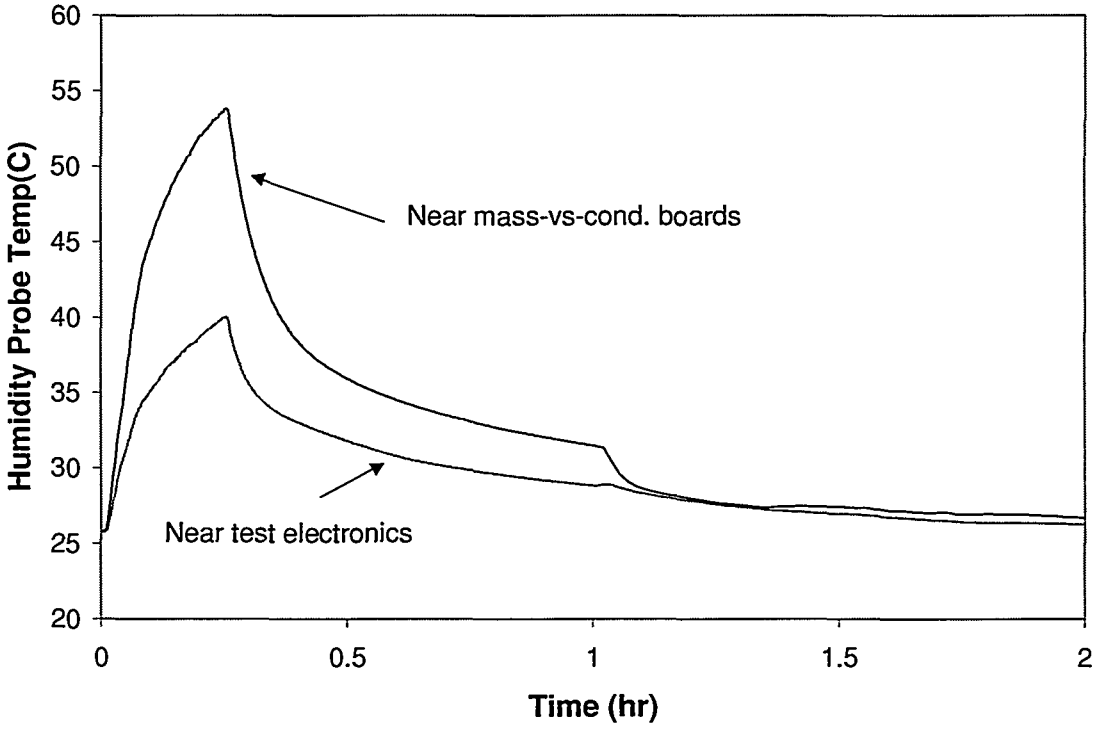

Figure 22. Temperature of the humidity probes in the smoke exposure chamber.

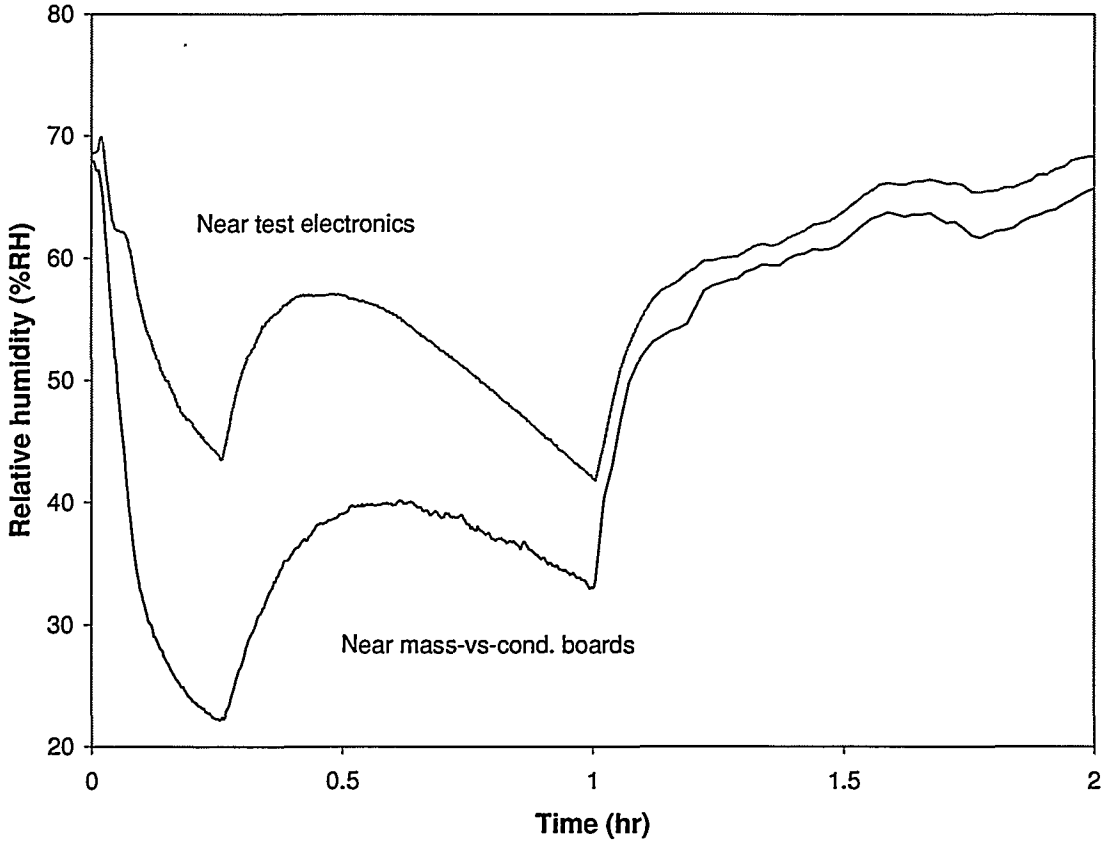

Figure 23. Relative humidity in two locations in the smoke chamber.

After 30 seconds the fuel began burning in the smoke chamber. Burning fuels that contain hydrogen (a characteristic of most organic fuels) creates water because the hydrogen molecules from the fuel material combine with oxygen to form H_2O. After 15 minutes, the lamps were turned off and the temperature of the smoke chamber dropped. At this point the RH increased slightly due to the drop in temperature, but since the nitrogen was still flowing, the RH did not recover to the level at which it started.

One hour after the lamps were turned on, the smoke chamber was vented. Smoke was pulled from inside of the smoke chamber to outside of the building with a hood and moist, 75% RH air replaced the smoke. Venting with high humidity air overcame the dry nitrogen bleed, and the RH in the chamber recovered to the original RH of the environmental chamber. By this time, most of the soot had precipitated from the air and attached to surfaces within the smoke chamber (including the surface of the RH sensor.)

Relative humidity is the ratio of water vapor to saturation water vapor. Relative humidity is a good measure of the effect of humidity on nearby materials such as antique books and tapestries, and is monitored to determine the effect of pollutants on conductivity of printed circuit boards. Another measure of humidity, the mixing ratio, reports how many grams of water are in the air compared to the kg of dry air.

The mixing ratio (Figure 24) is dependent on the temperature and pressure, since the air pressure determines how many kg of dry air is in a volume.[7] The mixing ratio shows the true effect of adding water vapor by burning and diluting the water vapor by adding nitrogen. The mixing ratio was calculated by estimating the ambient air pressure in the laboratory (approximately 1800 m above sea level) and calculating the mixing ratio of saturated air. Note that the humidity gage closest to the nitrogen feed by the mass-vs.-conductivity boards dropped faster after the lamps were turned off and remained lower than the gage further from the nitrogen feed until venting at 1 hour.

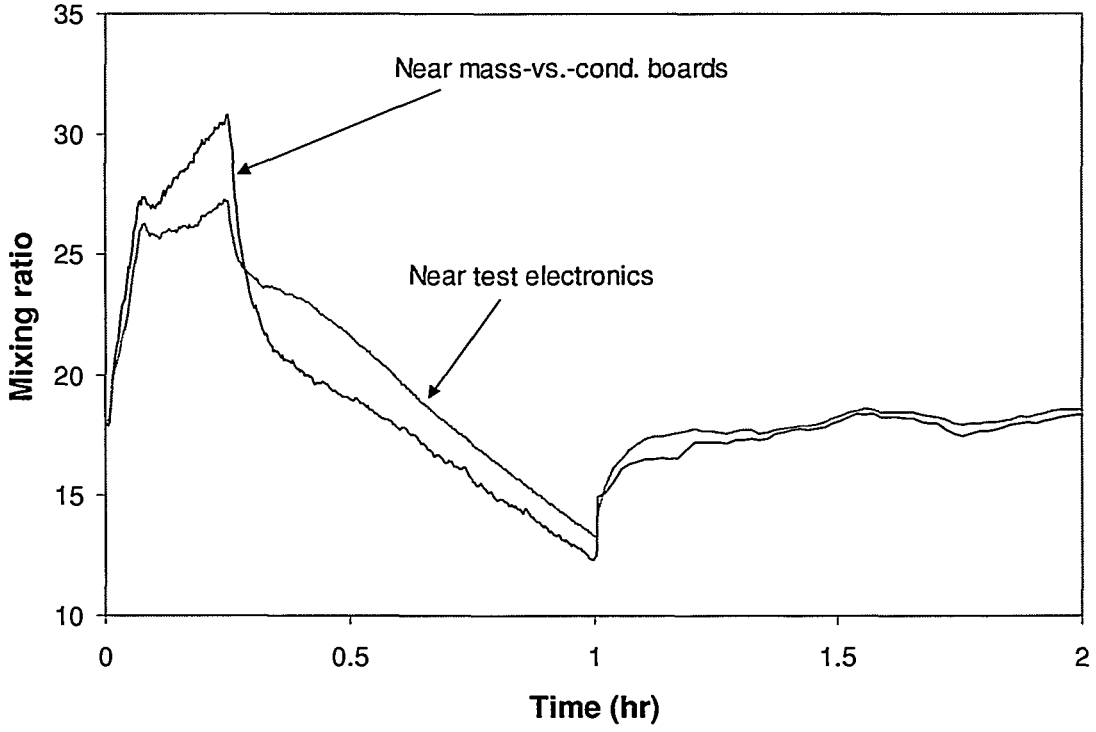

Figure 24. Mixing ratio (g of H_2O/kg air) during smoke test.

Conductance of soot-laden boards depended on both the suspended soot and the humidity. When the lamps were on and the optical density was significant, the conductance was dominated by any smoke deposited on the circuit boards. Later, after most of the deposition had occurred, changes in RH determined the changes in the conductance measured by the mass-vs.-conductivity boards. Figure 25 shows the conductance of the 500-Vdc biased board. The initial peak occurs while smoke was being generated and was in the air. After the initial peak, the conductance drifted down as the smoke in the air had settled, but the dry nitrogen was diluting the humidity. The nitrogen feed is located directly above the conductivity boards. After 1 hour, plastic plates were placed over these boards to reduce the loss of soot though venting action, and the smoke chamber was vented. The increases in conductance at this time mirror the increase in RH after the 1-hour period. Thus,

the conductivity boards reacted to the change in humidity once soot was deposited on the boards, as well as the smoke that was in the air.

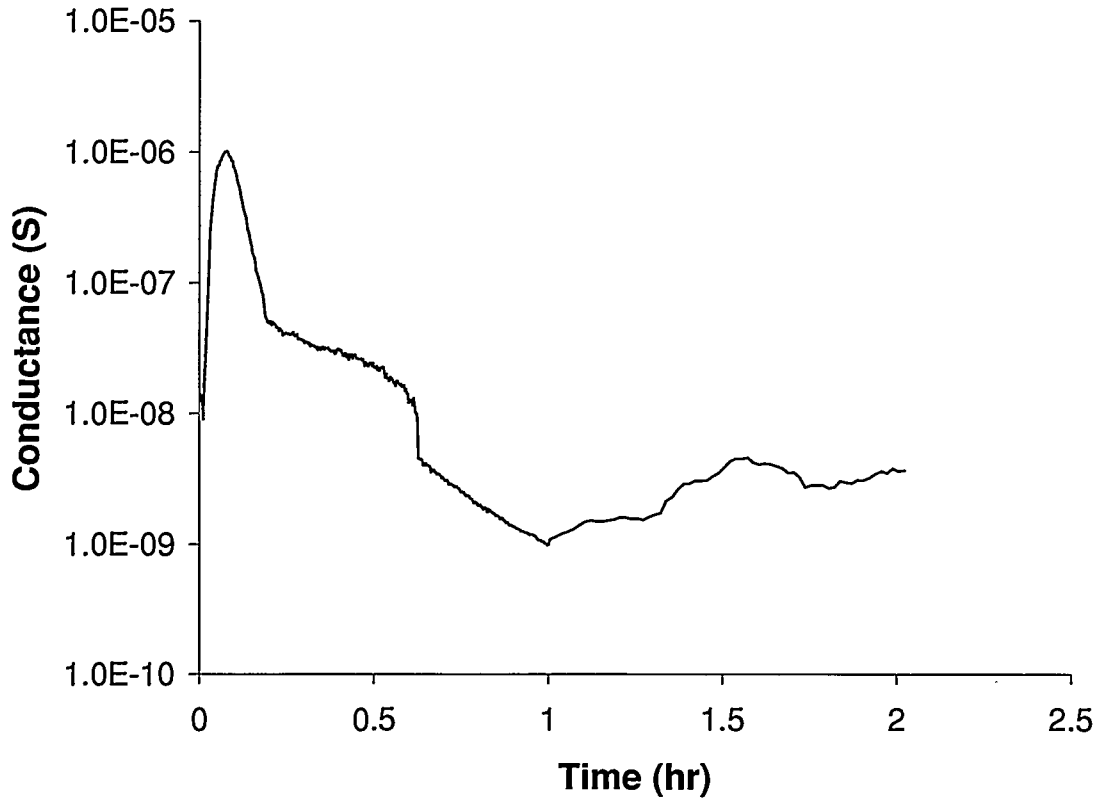

Figure 25. The conductance of the 500-Vdc biased mass vs. conductivity board.

3.6 Effect on different components

The throughput boards were unaffected by smoke. A simple test with a variable resistor indicated that the resistance between leads had to drop below 200 Ohms before any of the throughput signals would be interrupted.

The surface insulation measurements (with 5 V dc bias) were inconsistent as were the 5 Vdc-biased parallel plate. These voltages may have been too low to attract soot. The ac-biased plates displayed some changes in admittance at frequencies above 3 MHz.

None of the digital connectors failed. An evaluation of the likelihood of failure using a variable resistor in place of smoke showed that the conductance through the smoke must be very high, about 10^{-2} S, before the typical connector fails with this application. Most of our measurements of conductance indicate that a typical value with the smoke is about 10^{-6} S.

Some of the memory chips failed the functional test (after the fire was out and after the smoke was vented for fairly high smoke densities). The memory chips did not fail permanently. The chips that were tested with clean cables days or weeks after the smoke exposure passed the functional test. Parametric measurements did not necessarily indicate functional failure. The leakage current measurements indicate a peak during the fire; however, functional failure occurred well after the leakage currents fell to a normal range. The current injection measurement did indicate a difference during the functional failures. The reason for the functional failures after the smoke was vented is not known.

The smoke caused the memory chips to fail functionally. As shown in Figure 26, the 3.3V SRAM chip failed each of the four times it was tested with more than 10 g of fuel burned, but did not fail when less fuel was burned. The 5 V SRAM failed half of the time when more than 10 g of fuel was burned, but not for less fuel. The EPROMs failed once each at low fuel levels, but did not fail for higher levels. All of the chips were tested outside of the smoke after the test several weeks after the smoke exposure, and they all performed well. The failure of the memory chips was a temporary failure that occurred during or immediately after exposure to smoke.

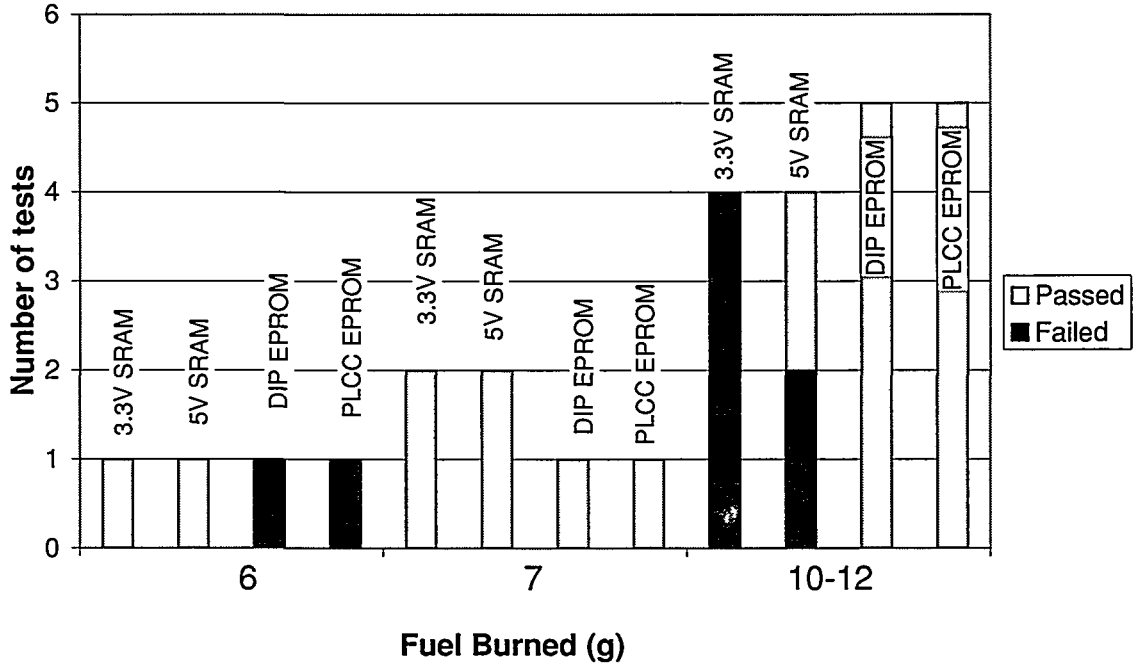

Figure 26. SRAM and EPROM chip results.

During the smoke exposure, the functional tests were performed every 30 seconds throughout the 2-hour smoke exposure test and recorded. Failures occurred at different times during the tests depending on the type of chip. A majority of the failures occurred after the smoke was vented. After venting, the test samples had a

coating of soot on them, but no additional soot accumulated. The environment was at 75 °F and 75% RH. Air was constantly circulated inside of the smoke chamber. The humidity level may have changed, but the change was not measured. On one hand, fire creates water when hydrocarbons are burned, but the slow nitrogen bleed used to protect the optical density lenses lowered the humidity level during the test.

The failures for lower smoke levels for the EPROMs are suspect data. The failure of the PLCC EPROM only occurred 2 times out of the 800 or more functional tests performed. The DIP EPROM failed more regularly; however, the first failures occurred before the smoke was added to the chamber and may have been caused by an improper test setup.

Parametric measurements were made of the chip characteristics while in the smoke. These parametric measurements did vary during the test, depending on how much smoke was introduced. As expected, leakage currents increased during the fire and were observed during the parametric measurement of leakage current while a standard voltage was applied to the supply pin (V_{inp} measurement). However, changes in leakage current did not correlate with most of the failures. Instead, the current on the supply pin varied drastically during chip failure.

When the 3.3 V SRAM chips failed, they tended to increase in current. The normal operating current was approximately 4 to 6 mA, but when these chips failed their supply current increased to greater than 10 mA. When the 5 V SRAM chips failed, their operating currents dropped to half of their normal value. Because the EPROMs failed only once each, no trend can be assessed.

4 Conclusions

Smoke increases conductance and can cause failures in energized electronic equipment through shorts and arcs. Smoke-induced leakage currents are highest during a fire when smoke is in the air, and these currents decrease as smoke settles. Smoke is attracted to static electric fields (dc) and will deposit on high potential surfaces, building bridges between potential surfaces and making a direct connection that shorts the surfaces together. The soot bridges are fragile and decay from air movement, but if there is smoke in the air, more bridges will form. Higher voltages will make more rugged bridges because the higher voltages produce higher forces to hold the soot together. The conductivity that results from a certain amount of smoke in the air is not modeled simply by the smoke density, but is also dependent on the geometry of the surfaces, the electrical potential, and air currents that can break the soot bridges.

Since smoke is attracted to electric fields, the deposition of smoke around dc circuits depends on the voltage strength. Experiments with printed circuit boards show that soot tends to pile up around solder traces biased with 50 Vdc, but form an even distribution near 5-Vdc biased traces. As a result, the conductivity of the 5-V

surfaces is higher after the smoke has settled, because the even distribution of soot provides a more continuous path for leakage currents.

High voltage ac circuits are also more susceptible to arcing when smoke is present, but the smoke does not build up and deposit in the same way as for a dc circuit. The particles of smoke are charged and provide an arc path. For both dc and ac circuits, the conductivity is highest when there is a lot of smoke in the air. As the smoke settles, the conductivity then depends upon soot bridges and the deposition patterns on surfaces. Once the smoke has deposited on surfaces, the conductivity can be influenced by humidity. Higher humidity levels increase conductivity.

Electronic failure is highly dependent upon circuitry. High-impedance circuits are most likely to suffer as a result of increased leakage currents from smoke. Since input/output circuits, such as the throughput circuits that were tested, have relatively high current output and low input impedance, they are not easily affected by smoke and did not fail. CMOS memory chips did fail, but not as expected; they failed after the smoke was vented when the density was low rather than during their highest leakage currents. Further investigation of the effect of humidity shows that the failures after venting may have been caused by adding humidity into the smoke chamber while venting, and, thus, increasing the conductivity of the deposited smoke. Tests on the same chips weeks later showed that they worked again. Hard disk drives did not fail.

The intent of this program was to model smoke-induced conductivity to aid in prediction of the electronic failures due to smoke. The research here has shown that conductivity is not only dependent on the smoke density, but also on the electrical circuit. Conductivity depends on the voltage, the geometry of the equipment, smoke composition, and air movement. Smoke particle sizes vary and can agglomerate into some large particles that can short some small-featured electronics. The uneven distribution and large particle sizes contribute to the difficulty in modeling. Elevated humidity levels also contribute to conductivity and should be included in any model. Equipment failure is dependent on the amount of smoke present, the interaction of the electrical fields with the smoke (determining the smoke accumulation), and the tolerance of the electronics to leakage currents.

Modeling equipment failure will require more effort. These efforts should include methods to predict how much smoke will be produced, more experiments where conductivity is measured for a given amount of smoke and humidity, and modeling of smoke movement in the presence of electric fields.

5 References

[1] Tina J. Tanaka, "Effects of Smoke on Functional Circuits", NUREG/CR-6543, SAND97-2544, Sandia National Laboratories, Albuquerque, NM, 1997

[2] Barbara Reagor, "Smoke Corrosivity: Generation, Impact, Detection, and Protection," Fire Sciences, v. 10, pp. 169-179, 1992

[3] Loren M. Caudill, J. T. Chapin, R. B. Commizzoli, P. Ghandi, G. A. Peins, and J. D. Sinclair, "Current State of Fire Corrosivity Testing: Preliminary Electrical Leak Current Measurements," in *Proc. International Wire and Cable Symposium*, pp.432-437, Army Communications Electronics Command, Fort Monmouth, NJ, 1995.

[4] T. J. Tanaka, S. P. Nowlen, and D. J. Anderson, "Circuit Bridging of Components by Smoke", NUREG/CR-6476, SAND96-2633, Sandia National Laboratories, Albuquerque, NM, 1996.

[5] Kofi Korsah, T. J. Tanaka, T. L. Wilson, Jr., and Richard T. Wood, "Environmental Testing of an Experimental Digital Safety Channel", NUREG/CR-6406, ORNL/TM-13122, Oak Ridge National Laboratory, Oak Ridge, TN, 1996

[6] Doug Pauls, "IPC Cleaning and Cleanliness Test Program Phase 3 Water Soluble Fluxes Part 1," Paper presented at the IPC 1992 Fall Meeting, October 12-15, 1992, Minneapolis, MN, Institute for Interconnecting and Packaging Electronics Circuits, Lincolnwood, IL, IPC TP-1043.

[7] Adolf S. Jursa, Editor, *Handbook of Geophysics and the Space Environment*, Air Force Geophysics Laboratory, Air Force Systems Command, United States Air Force, 1985.

DISTRIBUTION

AEA Technology
Attn. Keith W. McMinn
Winfrith Dorchester
Dorset DT 2 8DH
UK

Cardington Laboratory
Sue Rogers
No. 2 Hangar
Shortstown Bedford MK42 OTF
UK

HM Nuclear Installations Inspectorate
Attn: Paul A. Woodhouse
St. Peters House; Stanley Precinct
Balliol Road; Bootle
Merseyside L20 3LZ
UK

Interscience Communications Ltd.
Attn. Stephen J. Grayson
24 Quentin Rd.
London SE13 5DF
UK

Fire Testing Technology Ltd.
Attn. Gary Richardson
PO Box 116
East Grinstead
West Sussex RH19 3 GZ
UK

BT Networks and Systems
Attn: Jon Nixey
Building/Room B54/65
Martlesham Heath
IPSWICH
Suffolk IP5 3RE
UK

Centre Scientifique et Tech. du Batiment
Attn: Xavier Bodart
Station de Recherche
84 Avenue Jean-Jaures-Champs-sur-Marne
77428 Marne-La-Valle Cedex 2
FRANCE

Commisariat A L'Energie Atomique
Attn. Guy Gauthier
Institute of Protection and Nuclear Safe
B.P. 6 F - 92265
Fontenay-Aux-Roses Cedex
FRANCE

Institute de Protection et de Sûreté Nucléaire
Attn: Rémy Bertrand
CEA B.P. 6y-92265
Fontenay-Aux-Roses, Cedex
FRANCE

Electricite de France
Attn: Bernard Gautier
6 Quai Watier
78401 Chatou Cedex
FRANCE

Electricite de France
Attn: Maurice Kaercher
12-14 avenue Dutrievoz
69628 Villeurbanne Cedex
FRANCE

Societe Bertin & Cie
Attn: Serge Galant
BP No. 3
78373 Plaisir Cedex
FRANCE

University of Applied Sciences
ATTN: Prof.Dr.-Ing. Heinz-Willi Brenig
Department Insurance Studies
Secretariat
Mainzer Straβe 5
50678 Cologne
GERMANY

Gesamthochschule Kassel
Attn: Prof. U. H. Schneider
Institut fur Baustofflehre und Bauphysik
Technische Universität Wien
Karlsplatz 13, A-1040 Wien
GERMANY

Gesellschaft fur Reaktorsicherheit
Attn: Herr H. Liernersdorf
Schwertnergasse 1
D-5000 Koln 1
GERMANY

Institut fur Baustoffe,
Massivbau und Brandschutz
Jurgen Will
Beethovenstraβe 52
38106 Braunschweig
GERMANY

Koning und Heunisch
Attn: Dietmar Hosser
Lezter Hasenpfach 21
6000 Frankfurt/Main 70
GERMANY

Siemens AG - Ön QE 3
Attn: Dr. Karlheinz Frentzel
Hofmannstraße 51
D-81359 München
GERMANY

Hitachi Plant Eng. & Const. Co.
Attn: Dr. Kenji Takumi
Imai-Mitsubishi Bld. 5F
3-53-11 Minami-Otuska Toshima-Ku
Tokyo 170
JAPAN

National Research Institute of Fire and Disaster
Attn. Hiroshi Koseki
14-1 Nakahara 3
3 Chome
Mitaka, Tokyo 181
JAPAN

NUPEC
Attn: Dr. Hideo Ogasawara
Shuwa-Kamiyacho Bld.
3-13, 4-Chome
Toranomon, Minatoku
Tokyo 105
JAPAN

INER AEC R.O.C.
Attn: Su-Ji Sheu
1000 Wenhua, Rd.
Tzoyuan
Taiwan, R.O.C

Institute of Nuclear Energy Research
Attn: Andrew Tzeng
PO Box 3-11
Lung-Tam 325
Taiwan

Kopec
Attn: Jung Chang Na
360-9 Mabuk-Ri Kusung-Myun
Yongin-Si 449-910
SOUTH KOREA

Digital Institute of Nuclear Safety
Attn: Kim Bok Ryul
P.O. Box 114
Yosond Daejon 305-600
SOUTH KOREA

Korea Advanced Institute of Science and
Technology
Attn. Poong Hyun Seong
373-1 Kusong-Dong
Yusong-gu
Taejon 305-701
SOUTH KOREA

Ontario Hydro
Attn. S. Y. Lee
700 University Ave. H16 E01
Toronto, Ontario M5G 1X6
CANADA

Swedish National Testing and Research Institute
Attn. Soren Isaksson
Brinellgatan 4, Box 857
S-501 15 Boräs
SWEDEN

Swedish National Testing and Research Institute
Attn: Margaret Simonson
Brinellgatan 4, P.O. Box 857
S-501 15 Boräs
SWEDEN

Sycon Energikonsult
Attn: Fredrik Jorud
S-205 09 Malmo
SWEDEN

VTT Rakennustekniikka
Attn: Olavi Keski-Rahkonen
PO Box 1803
FIN-02044 VTT
FINLAND

VTT Rakennustekniikka
Attn: Matti Kokkala
PO Box 1803
FIN-02044 VTT
FINLAND

Fortum Engineering, Ltd.
Attn: Matti Lehto
POB 10, 00048 FORTUM, Finland
Rajatorpantie 8, Vantaa

Mika Yli-Kauhaluoma
Teollisuuden Voima Oy
27160 Olkiluoto
FINLAND

State of Israel, Ministry of Defense
Attn: Iiran Yrushalmi
P.O. Box 7192
Tel-Aviv 61071
ISRAEL

Arizona Public Service
Attn: Michael Scott
13928 N 78th Ave
Peoria, AZ 85381

Bell Atlantic Science & Technology, Inc.
Attn: Frank Terlato
140 West Street, 8th Floor Room 810
New York, NY 10007

Bell Atlantic Science & Technology, Inc.
Attn: L. C. Graff
140 West Street, 8th Floor Room 810
New York, NY 10007

Brookhaven National Laboratory
Attn: Mahbubul Hassan
P.O. Box 5000, Bldg 130
Upton, NY 11973

Capital Controls Company
Attn: Robert M. Taylor
3000 Advance Lane
Colmar, PA 18915

Copper Mountain Networks, Inc.
Attn: Tom Lavka
3931 Sorrento Valley Boulevard
San Diego, CA 92121-1402

DSC Communications Corporation
Attn: Alan Lewis
1000 Coit Road
Plano, TX 75075-5813

Department of Energy
Attn. Dennis Kubicki
19901Germantown Rd.
Germantown, MD 20874-1290

Duke Power
Attn. Michael H. Miller
Oconee Engineering
ONO2EE
PO Box 219
Seneca, SC 29679

DuPont Fluoroproducts
Attn. James. T. Walnock
Chestnut Run Plaza, 712
Wilmington, DE 19898

DuPont Polymers
Attn. Loren M. Caudill
Chestnut Run Plaza
Building 711
P. O. Box 80711
Wilmington, DE 19880-0711

DuPont Polymers
Attn. James R. Hoover
Chestnut Run Plaza, Bldg. 711
PO Box 80711
Wilmington, DE 19880

Electric Power Research Institute
Attn: Robert Kassawara
3412 Hillview Ave.
Palo Alto, CA 94303

Elf Atochem North America Inc.
Attn: Richard J. Rockosi
2000 Market St.
Philadelphia, PA 19103-3222

Factory Mutual Research
Attn. Dr. Erdem A. Ural
1151 Boston Providence Turnpike
P. O. Box 9102
Norwood, MA 02062

Factory Mutual Research
Attn. A. Tewarson
1151 Boston Providence Turnpike
P. O. Box 9102
Norwood, MA 02062

Factory Mutual Research Corporation
Attn: Jeff Newman
1151 Boston-Providence Hwy.
Norwood, MA 02062

Factory Mutual Engineering
Attn: Dr. Dimitrios Karydas
P.O. Box 9102
Norwood, MA 02062

Factory Mutual Research Corporation
Attn: Dr. Robert G. Bill, Jr.
P.O. Box 9102
Norwood, MA 02062

Fire Science and Technlogy Inc.
Attn. Vytenis Babrauskas
9000 300th Place SE
Issaquah, WA 98027

Federal Aviation Administration
Attn: Richard E. Lyon
William J. Hughes Technical Center
Atlantic City International Airport, NJ 08405

GBH International
Attn. Marcelo M. Hirschler
38 Oak Road
Rocky River, OH 44116

Hewlett-Packard Co.
Attn: Frank D. Dembski, Jr.
8000 Foothills Boulevard, MS 5619
Roseville, CA 95747-5619

Hughes Associates
Attn: Larry McKenna
3610 Commerce Dr., Suite 817
Baltimore, MD 21227-1652

Houston Advanced Research Center
Attn: David Norton
4800 Research Forest Drive
The Woodlands, TX 77381

Johns Manville
Attn: Steven Volenec
10100 W. Ute Ave. (80127)
P.O. Box 625005
Littleton, CO 80162-5005

Lockheed Martin Energy Systems
Attn. M. D. Muhlheim
Engineering Technology Division
Lockheed Martin Energy Systems
PO Box 2009
Oak Ridge, TN 37831

Lucent Technologies
Attn. J. D. Sinclair
Materials Reliability and Electrochemistry
Room 1D-259
600 Mountain Ave.
Murray Hill, NJ 07974

Lucent Technologies
Attn. R. B. Comizzoli
Process Reliability and Contamination Studies
Room 1E-217
600 Mountain Ave.
Murray Hill, NJ 07974

Lucent Technologies
Attn. J. T. Chapin
Room 2G52
2000 Northeast Expressway
Norcross, GA 30071

MDM Engineering Corp
Attn: Edward Quinn
23268 Atlanth Way
Dana Point, CA 92629

MET Laboratories
Attn: Troy Franklin
914 W. Patapsco Avenue
Baltimore, MD 21230-3432

MPR Associates Inc.
Attn: Douglas Chapin
320 King St
Alexandria, VA 22314-3238

National Academy of Sciences
National Research Council
Attn. Tracy D. Wilson
Board on Energy and Environmental System
2101 Constitution Ave. NW
Washington, DC 20418

Naval Surface Warfare Center
Attn. Usman Sorathia
Annapolis Detachment, Code 643
1662 Bay Head Rd.
Annapolis, MD 21401

NIST
Attn: Nora Jason
Fire Research Information Serv.
Building and Fire Research Laboratory
Gaithersburg, MD 20899

NIST
Attn: Rick Guann
Bldg 235 Rm A141
Gaithersburg, MD 20899

NIST
Attn: Dr. George W. Mulholland
Building 224, Room B-360
Gaithersburg, MD 20899

Nuclear Power Group
Attn: Dr. Joseph Naser
3412 Hillview Avenue
Palo Alto, CA 94303-1395

Oak Ridge National Laboratory
Attn. Kofi Korsah
PO Box 2008
Oak Ridge, TN 37831

Oak Ridge National Laboratory
Attn. Richard T. Wood
Reactor Systems Section
P.O. Box 2008, MS 6010
Oak Ridge, TN 37831

Oak Ridge National Laboratory
Attn. Paul D. Ewing
RF and Microwave Systems
P.O. Box 2009 MS 6006
Oak Ridge, TN 37831

Ohio State University
Mechanical Engineering Department
Attn: D.R. Miller
206 W. Eighteenth Ave
Columbus, OH 43210

Omega Point Laboratories
Attn. Arthur F. Grand
Director of Research
16015 Shady Falls Rd.
Elmendorf, TX 78112

Pratt & Whitney
Attn: Ernesto Suarez
P.O. Box 109600, MS 716-87
West Palm Beach, FL 33410

Product Safety Corporation
Attn. Carlos J. Hilado
P.O. Box 13080
Sissonville, West Virginia 25360

Roux International, Inc.
Attn. Henry J. Roux
PO Box 1513
Lancaster, PA 17603

Scientech, Inc.
Attn. Frank M. Quinn
11140 Rockville Pike, Suite 500
Rockville, MD 20852

Schirmer Engineering Corporation
Attn: Stephen M. Hill
2009 N. 14th St., Suite 100
Arlington, VA 22201-2514

South Hills Datacomm
Attn: Matthew Huffmyer
760 Beechnut Drive
Pittsburgh, PA 15205

Southwest Texas State University
Attn: Joseph H. Koo
601 University Drive
San Marcos, TX 78666-4616

Southwire
Attn. Buddy Powers
1 Southwire Drive
Carrollton, Georgia 30119

The Govmark Organization, Inc.
Attn. Samuel Sadinsky
PO Box 807
Bellmore, NY 11710

The Pennsylvania State University
Attn. Stephen J. Kenney
Department of Nuclear Engineering
231 Sackett Building
University Park, PA 16802

The RM Group
Attn: Ron Moore
12024 Broadwood Drive
Knoxville, TN 37922

U.S. Department of Energy
Office of Scientific and Technical Information
P.O. Box 62
Oak Ridge, TN 37831

U.S. Department of the Navy
Attn: M. Allen Matteson
David M. Taylor Naval Ship Research and
Development Center
Mail Code 1740.2
Bethesda, MD 20084-5000

U.S. Department of the Navy
Attn: David Satterfield
National Center #4, Room 311
Naval Sea System Command (56Y52)
Washington, DC 20362

Underwriters Laboratories
Attn: Pravinray Ghandi
333 Pfingston Rd.
Northbrook, IL 60062

Underwriters Laboratories
Attn: Robert Backstrom
333 Pfingston Rd.
Northbrook, IL 60062

University of California
Attn. Dr. Carlos Fernandez-Pello
Mechanical Engineering Dept.
6105a Etcheverry Hall
Berkeley, CA 94720

Vista Engineering, Inc.
Attn. Alexander R. Klein
69 Milk Street
Westborough, MA 01581

Wyle Laboratories
Attn: Don Davis
P.O. Box 077777
Huntsville, AL 35807-7777

U.S. Nuclear Regulatory Commission
Washington, DC 20555-0001

Christina Antonescu (3)
MS 10 L1

John Calvert
MS 10 L1

Erulappa Chelliah
MS 9 B3

Matthew Chiramal
MS 12 H2

Ed Connell
MS 11 A11

Mark Cunningham
MS 10 E50

Joseph P. Joyce
MS 6 F2

Thomas L. King
MS 10 E50

Joel Kramer
MS 10 E46

Eric J. Lee
MS 12 H2

Pat Madden
MS 11 A11

Evangelos C. Marinos
MS 12 H2

Jerry L. Mauck
MS 12 H2

Frank J. Miraglia, Jr
MS 16 E15

Nathan Siu
MS 10-E50

Ashok C. Thadani
MS 10 F12

Jit P. Vora
MS 10 E10

Jared S. Wermiel
MS 10 B3

Steven West
MS 11 F1

Internal

MS	Org	Name
1129	6428	Tina J. Tanaka (20)
0744	6420	Edward Baynes, Jr.
0748	6413	S.P. Nowlen
0836	9117	John Brockmann
0836	9116	Lou Gritzo
9052	8361	Christopher Shaddix
0836	9116	Vern Nicolette
0746	6613	Dennis J. Anderson
0746	6613	Robert M. Cranwell
0744	6400	Dana Powers
0553	9116	Walt Gill
9018	8940-2	Central Technical Files
0899	4916	Technical Library (2)
0612	4912	Review and Approval Desk For DOE/OSTI
0188	4001	LDRD Office